NUMERICAL MODELING OF TWO-DIMENSIONAL TEMPERATURE DYNAMICS ACROSS ICE-WEDGE POLYGONS

By

Viacheslav V. Garayshin, B.S., M.S.

A Thesis Submitted in Partial Fulfillment of the Requirements

for the Degree of

Master of Science

in

Geophysics

University of Alaska Fairbanks

May 2017

APPROVED:

Vladimir Romanovsky, Committee Chair
Alexei Rybkin, Co-Chair
Dmitry Nicolsky, Committee Member
Larry Hinzman, Committee Member
Paul McCarthy, Chair
Department of Geosciences
Paul Layer, Dean
College of Natural Science and Mathematics
Michael Castellini, *Dean of the Graduate School*

Abstract

The ice wedges on the North Slope of Alaska have been forming for many millennia, when the ground cracked and the cracks were filled with snowmelt water. The infiltrated water then became frozen and turned into ice. When the annual and summer air temperatures become higher, the depth of the active layer increases. A deeper seasonal thawing may cause melting of ice wedges from their tops. Consequently, the ground starts to settle and a trough begins to form above the ice wedge. The forming trough creates a local temperature anomaly in the surrounding ground, and the permafrost located immediately under the trough starts degrading further. Once the trough is formed, the winter snow cover becomes deeper at the trough area further degrading the permafrost.

In this thesis we present a computational approach to study the seasonal temperature dynamics of the ground surrounding an ice wedge and ground subsidence associated with ice wedge degradation. A thermo-mechanical model of the ice wedge based on principles of macroscopic thermodynamics and continuum mechanics was developed and will be presented. The model includes heat conduction and quasi-static mechanical equilibrium equations, a visco-elastic rheology for ground deformation, and an empirical formula which relates unfrozen water content to temperature. The complete system is reduced to a computationally convenient set of coupled equations for temperature, ground displacement and ground porosity in a two-dimensional domain. A finite element method and an implicit scheme in time were utilized to construct a non-linear system of equations, which was solved iteratively. The model employs temperature and moisture content data collected from a field experiment at the Next-Generation Ecosystem Experiments (NGEE) sites in Barrow, Alaska. The model describes seasonal dynamics of temperature and the long-term ground motion near the ice wedges and helps to explain destabilization of the ice wedges north of Alaska's Brooks Range.

Table of Contents

List of Figures

Page

List of Tables

Page

Acknowledgements

I would like to express my gratitude to committee members Dr. Vladimir Romanovsky, Dr. Alexei Rybkin, Dr. Dmitry Nicolsky and Dr. Larry Hinzman as well as to others who helped me with my admission and study.

First, I am grateful to Dr. Alexei Rybkin for recommending me for the Geophysics study program; Vladimir Romanovsky and admission committee members for accepting me into the program under financial assistance. While pursuing my degree in Geophysics under the supervision of Dr. Vladimir Romanovsky, I was able to gain professional skills which will likely allow me to obtain an interesting job. Also, while being an international student I was happy to create my own nuclear family in this beautiful part of the world named Alaska.

Second, I am thankful to my committee member Dmitry Nicolsky for his clever guidance of me through all the steps of my study program. In particular he guided my learning of numerical methods, mechanics and development of the thermo-mechanical model. Also, he helped me with a rheological model for simulation of ground subsidence. I am grateful to Dr. Vladimir Romanovsky and Dr. Dmitry Nicolsky for being patient with me and helping me to prepare for and go to the AGU conference in December 2016, where I presented preliminary results of my thesis work. Attending this scientific conference, I obtained a unique life experience. Also, I appreciate the advise given by Dr. Larry Hinzman about how to give good presentations and his encouragement to be self-motivated in my study and work.

I would like additionally to thank William Cable for providing data for soil temperatures and snow characteristics from the study site in Barrow, Alaska. In particular I want to thank him for sharing 2-D thermal snapshots of ice wedge polygon cross-section with me, and for clearing snow cover data obtained at the study site from observational noise.

Finally, I am grateful to my wife Sharon Carrasquillo Torres for believing in my success and helping me with maintaining my study progress.

Introduction

Different environmental observations and studies summarized by *Serreze et al.* (2000) show an acceleration of climate warming in high northern latitudes since the 1970s. This acceleration triggered observable changes in many ecosystems (*Walther et al.*, 2002) and permafrost (*Schaefer et al.*, 2012). *Jorgeson et al.* (2006) indicate an acceleration of permafrost degradation in Alaska since the early 1980s with observed changes in the Alaskan Arctic mainly occurring along ice wedges. Melting of ice causes differential ground settlement and produces ground surface depressions causing formation of pits and gullies (*Osterkamp et al.*, 2009). Furthermore, a significant degradation of ice wedges causes formation of thermokarst ponds and lakes (*Jorgeson et al.*, 2006; *Raynolds et al.*, 2014), leading to drastic changes in hydrology. Changes in hydrology (*Walvoord and Striegl*, 2007; *Liljedahl et al.*, 2012) consequently lead to changes in water drainage (*Fortier et al.*, 2007; *McGraw*, 2008), and then to alternations in transportation of sediments and dissolved nutrients, which further affect vegetation and biological production in arctic streams (*Bowden et al.*, 2008). With the thawing of ice-rich permafrost, the ground becomes more prone to active layer detachments (*Lewkowicz*, 2007) and to retrogressive thaw slumps (*Burn and Lewkowicz*, 1990; *Lantz and Kokelj*, 2008). Additionally, thawing of ice-rich permafrost through ice wedge degradation, ground deformation and flooding causes damage to infrastructure (*USARC*, 2003), particularly to roads, houses and pipelines (*Osterkamp et al.*, 1997). According to data presented in *USARC* (2003) areas where the volumetric excess ice content is at least 10% cover most of the North Slope and Interior Alaska.

Currently, a significant amount of research into thermokarst development has already been conducted. In particular, a study of thermokarst development through in-situ measurements of ground subsidence, soil densities and ground-ice volumes was conducted by *Osterkamp et al.* (2009) near Healy; field surveys combined with the analysis of aerial photos were used by *Jorgeson et al.* (2006) for studying the ice wedge degradation across Alaska's Arctic and by *Raynolds et al.* (2014) to show thermokarst development in the Prudhoe Bay area. Besides observational approaches, thermokarst development has been actively studied through modeling.

The first known numerical model of thermokarst development was published by *Hinzman et al.* (1997). In this model ground settles because of the reduction of ice volume upon thawing and drainage of excess water. Drainage of excess water in this model occurred instantly upon thawing of ice rich permafrost, and the amount of excess water was determined from the postdrainage value of porosity. Depth of thawing was determined from ground temperature dynamics estimated through solving a 2-D heat conduction equation with phase change and applying a developed model of surface energy balance. The heat conduction equation was solved using a fixed grid finite element

method. Later, *West and Plug* (2008); *Plug and West* (2009) and *Wen et al.* (2016) developed numerical models predicting evolution of bathymetry of thermokarst lakes. A thermokarst lake was developing upon the thawing of underlying ice-rich permafrost. Similar to *Hinzman et al.* (1997) thawing of permafrost was predicted through the solving of the 2-D heat conduction equation with the phase change. Thaw consolidation was assumed to occur instantly upon the thawing of excess ice under the bottom of the lake and the amount of excess water in each case was also determined from the introduced postdrainage value of porosity. *Plug and West* (2009) additionally included in their model the hillslope and mass movement processes which were parameterized by sediment transport relation, downslope movement rate and deposition rate. Different boundary conditions defining a temperature of ground surface or temperature of the lake water were introduced in all three works (*West and Plug*, 2008; *Plug and West*, 2009; *Wen et al.*, 2016), a finite difference numerical scheme was used by *West and Plug* (2008) and *Plug and West* (2009) and a finite element method with a moving grid was used by *Wen et al.* (2016). A different numerical model of ground subsidence was proposed by *Lewis et al.* (2012). In their approach the ground subsided due to drainage of excess water upon permafrost thawing but drainage was assumed to occur through a route located at depth and the drainage rate was described by Darcy's law. The rate was controlled by water pressure and porosity of the ground and these properties depended on the amount of excess water defined through the postdrainage value of porosity. The ground deformation was assumed to occur continuously upon drainage, and the settlement due to other factors was neglected. The domain of the thawed ground was determined by solving the heat conduction equation with the phase change. The next generation of models included the influence of ground mechanical properties on the ground subsidence upon the thawing of permafrost. In particular, *Yao et al.* (2012), *Qi et al.* (2012) and *Wang et al.* (2015a,b) proposed a numerical model of large strain consolidation of thawing permafrost. In this model the balance of linear momentum, the elastic stress-strain relationship, and the Jaumann stress rate (*Dienes*, 1979) were employed to describe the mechanical behavior of soil. The soil skeleton was assumed to maintain its structure upon the consolidation while the flow of water through the soil was described by Darcy's law. The heat equation with the phase change was proposed to determine the boundary between thawed and frozen domains. The mass conservation equation was employed to consider a compressibility of fluid and solid particles.

In my thesis, I describe a thermo-mechanical model dedicated to the investigation of ice wedge degradation, which is associated with a trough formation. In my model I include the process of melting of ice wedges associated with a rise of air temperatures, a process of ground subsidence over melted wedges, and a feedback mechanism, between these processes and the ground thermal regime in ice wedge polygons. For simplicity I simulate these processes over a 2-D cross-section of an ice wedge. The temperature dynamics are estimated through solving the heat conduction

equation with the phase change. Water appearing after thawing of an ice wedge is assumed to drain instantly because of cracks in the ground. Deformation of the thawed ground above the melted part of an ice wedge is described by a linear viscoelastic Kelvin-Voigt model and the Cauchy equation of quasi-static equilibrium (*Holzapfel*, 2000). I also assume that the consolidation of soil is negligible and its skeleton maintains its structure upon deformation.

An outline of this thesis is as follows. In Chapter 1, I simulate temperature dynamics around a stable ice wedge. In particular in Section 1.1, I present a 2-D model of the heat transfer around an ice wedge, while in Section 1.2 I validate my simulations using some exact solutions. Section 1.3 deals with numerical simulations of temperature dynamics around an ice-wedge polygon near Barrow, Alaska. The input data for the heat transfer problem are obtained according to thermal properties of soil and ice in the polygon, and measured snow depth, and air temperature. Finally, I compare numerical results and temperature observation for the polygon and discuss the modeling results in Section 1.4. In Chapter 2, I investigate processes of ice wedge degradation and ground subsidence. In particular, in Section 2.1 I present a viscoelastic Kelvin-Voigt model of ground deformation around an ice wedge, coupled with the model of 2-D heat transfer. In Section 2.2, I validate simulations conducted with the Kelvin-Voigt model against exact solutions. In Section 2.3, I apply a coupled thermo-mechanical model to simulate the process of ice wedge degradation with trough formation. In the same section I investigate an effect of snow on the positive feedback mechanism between ice wedge degradation and ground subsidence, and an effect of the water table on these processes.

Chapter 1

Simulation of temperature dynamics around a stable ice wedge

1.1 Thermal model describing temperature dynamics of the ground around an ice wedge

Ice wedges are parts of a polygonal network of ice enclosing polygons or cells of frozen ground from 3 to 30 m or more in diameter (*Pewe*, 1963). Before proceeding further, I briefly recall the physical processes responsible for the formation of ice wedges. According to *de K. Leffingwell* (1915); *Lachenbruch* (1963); *Pewe* (1963) and *Erwin* (1963) ice wedges are specific forms of the massive ice in permafrost. A wedge grows when the ground thermally contracts during a cold winter and a vertical crack propagates downward below the frozen active layer into the permafrost (*Davis*, 2001). Water consequently fills a crack in the spring while the permafrost is still contracted. When water fills in the crack, it freezes and expands the ground material. This process may repeat the next winter and an ice wedge grows. Many ice wedges formed during a repetitive frost-cracking process, which may last from several decades up to thousands of years. In this study I do not model ice wedge development, but rather focus on an investigation of temperature regimes around existing ice wedges near the coast of the Arctic Ocean in Alaska.

An example of a group of ice wedge polygons is shown in Figure 1.1a. As one can see from Figure 1.1a, ice wedges are located at least several meters apart from each other. This allows me to assume that the temperature regime surrounding a particular wedge does not change significantly along the wedge, i.e. parallel to the contraction plane. Using this assumption I will model temperature dynamics across the wedge, i.e. perpendicular to the contraction plane. This cross-section is marked by a dashed line in Figure 1.1a and its sketch is presented in Figure 1.1b. I assume that the top of a wedge is located below the active layer, the wedge is $1-4$ meters across, at least several meters in lateral direction, and several meters downward. Since thermal properties of ice are different from thermal properties of the surrounding ground materials, ice wedges can produce local ground temperature anomalies. For the sake of simplicity in the numerical modeling I assume that an ice wedge is symmetric with respect to its contraction plane. This assumption is based on a symmetric appearance of exposed ice wedges shown in *de K. Leffingwell* (1915); *Pewe* (1963); *Mackay* (1974) and *Jorgeson et al.* (2006). I hence calculate temperatures only on one side of the contraction plane.

A sketch of the computational domain for an ice wedge cross-section is shown in Figure 1.2. Upper boundary BE represents the ground surface during the snowfree period. When snow is present this boundary is associated with the snow surface. Lower boundary AF is the ground at 30m depth,

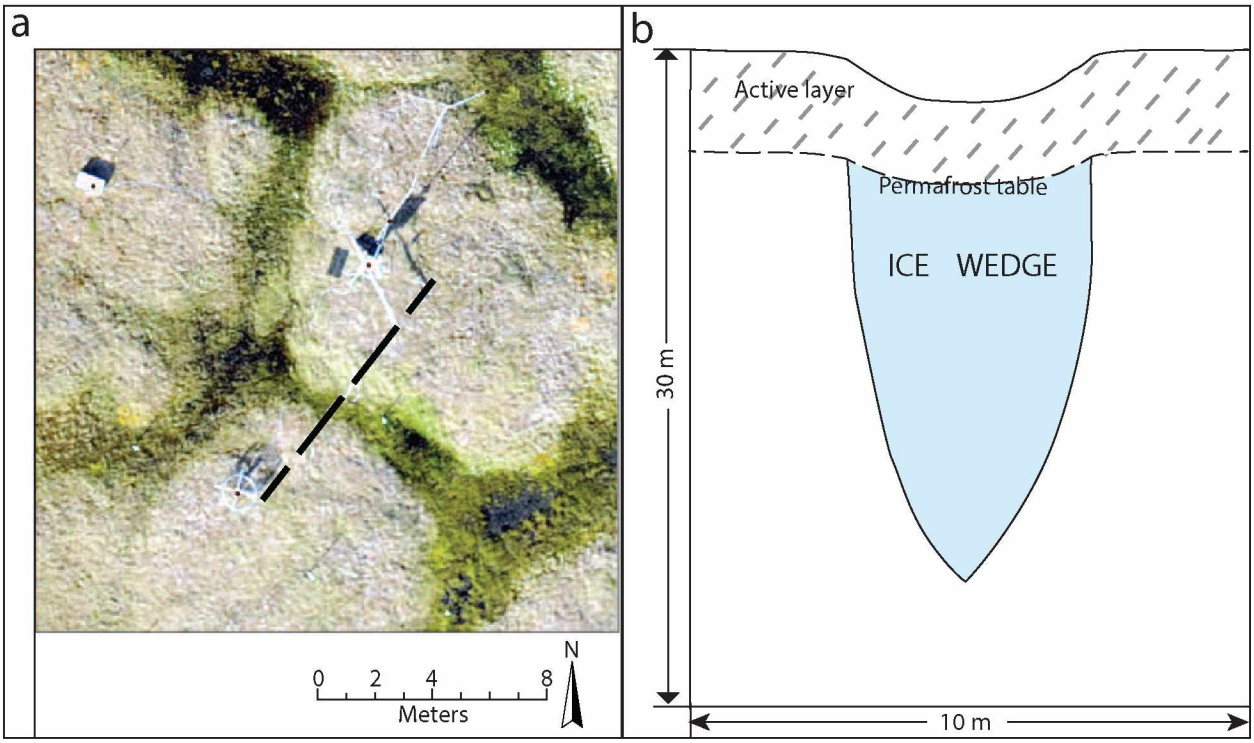

Figure 1.1: a) A view of high-centered ice wedge polygons near Barrow, Alaska, 71°17′N 156°36′W. The dashed line shows the surface trace of the cross-section. b) A schematic sketch of the ground cross-section containing an ice wedge.

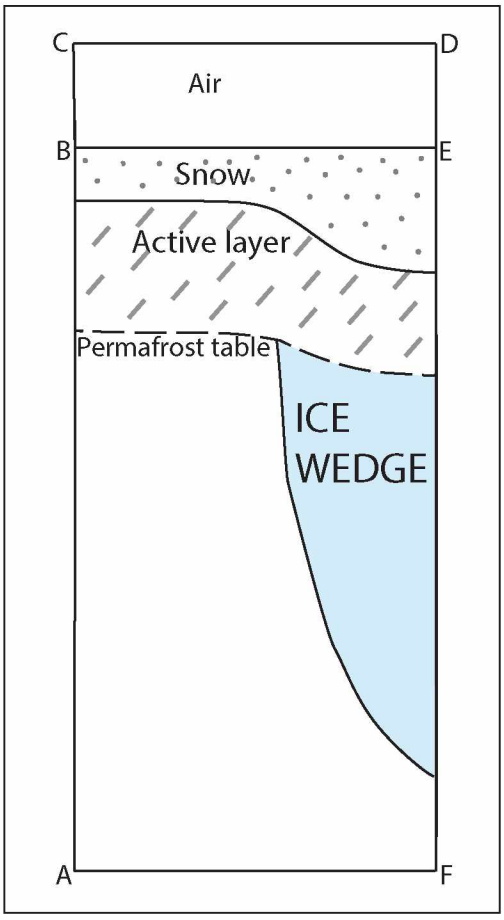

Figure 1.2: A sketch of the computational domain for simulation of temperature dynamics around an ice wedge.

where seasonal variations of temperature could be assumed to be negligibly small (*Brewer*, 1958). Left boundary AB is the center of an ice wedge polygon and the horizontal heat flux at AB is assumed to be zero. Right boundary EF coincides with the contraction plane of the ice wedge and due to assumed symmetry I assume zero heat flux through this boundary.

Supposing that migration of water and evaporation are not significant processes and that soil is fully saturated, I simulate temperature dynamics around the ice wedge by the 2-D heat equation with the phase change (*Carslaw and Jaeger*, 1959):

$$\left(C + L\frac{\partial \theta_w}{\partial T}\right)\frac{\partial T}{\partial t} = \nabla\left(\lambda \nabla T\right), \tag{1.1}$$

where $T = T(x, y, t)$ [K] is the temperature, $\nabla = (\partial/\partial x, \partial/\partial y)$ is the vector differential operator, x [m] and y [m] are horizontal and vertical coordinates describing a position in the ground material and snow, t [s] is time, $C = C(T, x, y)$ [J/(m$^3 \cdot$ K)] is the volumetric heat capacity of soil or snow, $\lambda = \lambda(T, x, y)$ [W/(m $\cdot$ K)] is the thermal conductivity of soil or snow; L [J/m^3] is the volumetric

latent heat of fusion of water and $\theta_w = \theta_w(T, x, y)$ [m^3/m^3] is the volumetric unfrozen water content of soil. I calculate the thermal conductivity λ and the volumetric heat capacity C for soil according to (*de Vries*, 1963) and as described in (*Sass et al.*, 1971; *Osterkamp*, 1987) and (*Nicolsky et al.*, 2007a).

$$\lambda(T) = \lambda_s^{\theta_s} \lambda_i^{\theta_i(T)} \lambda_w^{\theta_w(T)}, \tag{1.2}$$

$$C(T) = \theta_i(T) C_i + \theta_w(T) C_w + \theta_s C_s. \tag{1.3}$$

By letters i, w, and s, I abbreviate the properties of ice, liquid water and soil particles, respectively. The constants C_k and λ_k are the volumetric heat capacity and the thermal conductivity of the k-th constituent, $k \in \{i, w, s\}$, respectively. The quantity θ_k is the volume fraction of the k-th constituent such that $\theta_s + \theta_w + \theta_i = 1$. Since soil is fully saturated I derive that soil porosity η is equal to $\eta = \theta_w + \theta_i$. Moreover, since deformation of the soil skeleton is assumed to be negligibly small, η is assumed to be constant that depends on the soil type. For the sake of simplicity I approximate the thermal conductivity and the volumetric heat capacity for the snow cover by constants (*Goodrich*, 1982; *Romanovsky and Osterkamp*, 2000; *Zhang et al.*, 2001; *Mölders and Romanovsky*, 2006) and assume that the volumetric unfrozen water content for snow is zero (*Jafarov et al.*, 2014).

Numerical modeling experiments conducted by *Romanovsky and Osterkamp* (2000) lead to the conclusion that for successful modeling of freezing/thawing of the ground it is necessary to consider unfrozen water which is present in many types of soils at temperatures below 0°C (*Hobbs*, 1974). The volumetric unfrozen water content $\theta_w(T)$ is defined as a ratio of liquid water volume in a representative soil sample at temperature T to the total volume of the sample. Examples of introduced unfrozen content for soils are presented in Figure 1.3. There are different types of approximation to θ_w in the fully saturated soil (*Lunardini*, 1988; *Galushkin*, 1997). Here, I employ a smooth parametrization described by *Nicolsky et al.* (2009). This parametrization can be written as

$$\theta_w(T) = \eta [\phi(a, T^*, T)]^b, \tag{1.4}$$

where $a, b > 0$ are constants. The quantity $T^* < 0$°C is the freezing point depression (*Hobbs*, 1974), the maximal temperature for which ice exists in the ground, and $\phi(a, T^*, T)$ is the exponential function taking the value 1 for $T \geq T^*$ and values between 0 and 1 otherwise. The constant a is the regularization parameter ensuring that ϕ is continuously differentiable with respect to T.

Following *Zienkiewicz and Taylor* (1991), I employ the finite element method (FEM) with a fixed computational grid to solve the heat conduction equation (1.1). For calculation of the temperature dynamics an initial temperature distribution $T(x, y, 0) = T_0(x, y)$ is prescribed for the domain

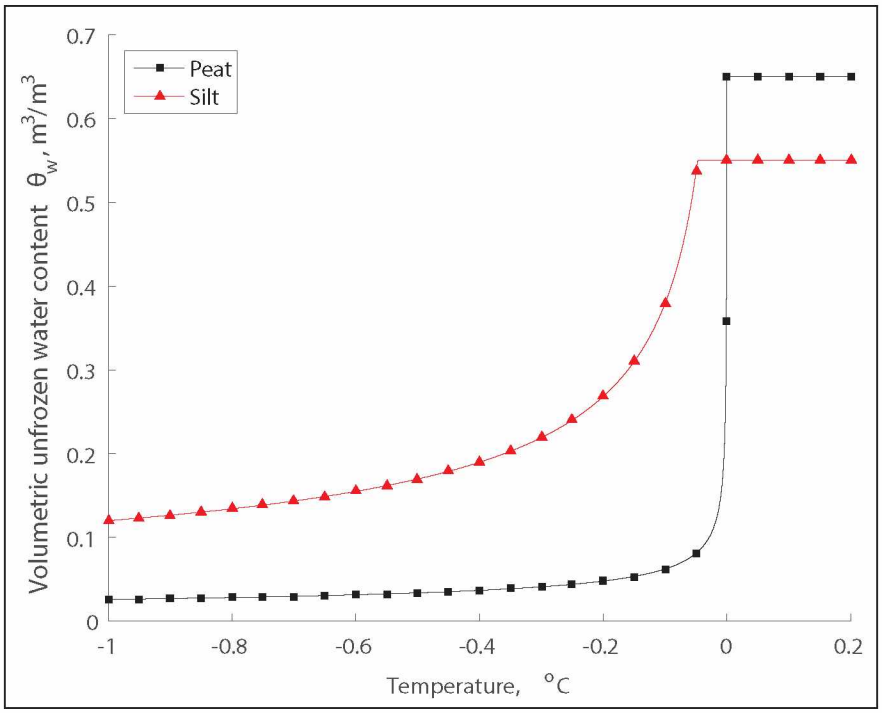

Figure 1.3: Parametrization of the volumetric unfrozen water content for the ground material near Barrow, Alaska (*Romanovsky and Osterkamp*, 2000).

$ABEF$ at time $t = 0$. Zero horizontal heat fluxes are assumed through both vertical boundaries AB and EF. A temperature regime $T(t)$ is prescribed for the upper boundary BE and a heat flux is set at the lower boundary AF. To parameterize variation of the snow cover, I embedded domain ABEF into larger fixed in time domain ACDF as shown in Figure 1.2. To implement the upper boundary condition associated with the temperature $T(t)$, this condition is assigned to each grid node of area $BCDE$ which is associated with the air. This method, when a moving domain is embedded into a larger fixed in time domain is called the fictitious domain method (*Glowinski et al.*, 1994). An important advantage of this method is that a time consuming element triangulation of domain ABEF could be avoided to represent changes of this domain associated with the variation of snow cover.

I implement the so-called lumped approach (*Zienkiewicz and Taylor*, 1991) with association of a control volume for each grid node to formulate the FEM matrices. The lumped formulation is chosen for handling possible stability and oscillations issues of the solution (*Pham*, 1995; *Nicolsky et al.*, 2007a). Another difficulty in numerical modeling of soil freezing/thawing is in consistent calculation of the derivative $d\theta_w/dT$ in equation (1.1) as discussed in (*Nicolsky et al.*, 2009). For coarse-grained materials function θ_w rapidly changes over a small temperature range near 0°C and this change can be easily miscalculated or even missed (*Pham*, 1986; *Comini et al.*, 1989). To avoid

this potential error I employ the enthalpy temporal averaging method (*Morgan et al.*, 1978) to calculate $d\theta_w/dT$. The resultant system of equation is discretized in time using the fully implicit Euler method. At each time step the equation is solved iteratively with a combination of Pickard iterations (*Kolmogorov and Fomin*, 1975) and the Newton method (*Kelley*, 2003). A convergence condition is checked at each iteration. If the convergence condition is not met, the time step is halved and the iterations are repeated.

1.2 Validation of the thermal model

In this section I validate my numerical scheme of the simulated heat transfer process. For this purpose I conduct a series of tests, called benchmarks. First, I compare numerical and analytical solutions for the temperature wave problem (*Tikhonov and Samarskii*, 1963) and then compare solutions for the classical Stefan problem (*Gupta*, 2003).

1.2.1 Benchmark Problem 1: Temperature wave

In this sub-section, I compare numerical and analytical solutions to the 1-D heat conduction problem with a periodic boundary condition at the surface and a geothermal gradient, the problem of propagation of temperature waves (*Tikhonov and Samarskii*, 1963). I consider an infinitely deep soil column with a flat surface and thermally insulated vertical sides and assume that ground thermal properties λ and C do not change with temperature and with depth, and volumetric unfrozen content of the ground $\theta_w = 0$. In this case the thermal regime can be calculated analytically at any depth as a function of periodic thermal regime at ground surface and the depth.

For validation of my numerical scheme I simulate temperature dynamics over a d = 30 m deep soil column shown in Figure 1.4. For the sake of simplicity, I assume a homogeneous soil column with thermal conductivity $\lambda = 2$ W/(m $\cdot$ K) and heat capacity $C = 2 \cdot 10^6$ J/(m^3 $\cdot$ K). At the upper boundary I prescribe temperature dynamics

$$T(t) = T_m + A\sin(2\pi t/\tau), \tag{1.5}$$

where $T_m = 25°$C is the mean annual temperature, $A = 20$ K is the annual amplitude, t [s] is the time, $\tau = 365$ days is the one year period. The value of the geothermal gradient G is assumed to be 0.03 K/ m. At the lower boundary $x =$ d I prescribe a vertical temperature gradient $\frac{\partial T}{\partial y}$. The analytical solution for the temperature gradient by (*Tikhonov and Samarskii*, 1963) is

$$T_y(t) = G + \sqrt{2}ABe^{B\mathrm{d}}\sin(2\pi t/\tau + \pi/4 + B\mathrm{d}), \tag{1.6}$$

Table 1.1: Discrepancies between numerical and analytical solutions for the temperature waves problem. For each combination $\{\Delta x, \Delta t\}$ the discrepancy is estimated as $\max_{(x,y,t)}\{T^{\text{num}} - T^{\text{an}}\}$, where T^{num} and T^{an} are numerical and analytical solutions for temperature dynamics respectively. The errors are presented in 10^{-1}K.

	$\Delta x = 0.5$ m	$\Delta x = 0.25$ m	$\Delta x = 0.1$ m
$\Delta t = 5$ days	2.32	2.16	2.12
$\Delta t = 2.5$ days	1.26	1.12	1.08
$\Delta t = 1$ day	0.64	0.48	0.44

where $B = -0.315 \pm 0.001$ is the phase lag increment per 1 m of depth. The heat fluxes through the lateral sides of the column equal zero. The initial temperature distribution $T_0(y)$ at the soil column also follows from the analytical temperature wave propagation solution at $t = 0$ as

$$T_0(y) = T_m + A \cdot e^{By} \sin(By). \tag{1.7}$$

After prescribing boundary and initial conditions I computed temperature dynamics over uniform grids with grid sizes $\Delta x = 0.1$, 0.25 and 0.5 m. For simplicity I assume that the width of the computational domain w is equal to Δx. For each grid the simulations are handled with different time steps $\Delta t = 1$ day, 2.5 days and 5 days. Every numerical solution is obtained over one year period τ and is compared with the analytical result.

For each combination of $\{\Delta x, \Delta t\}$ I list the discrepancies between numerical and analytical solutions estimated over an entire grid and an entire year of simulation in Table 1.1. The values show that with decrease of both Δx and Δt, the error between analytical and numerical solutions decreases as well. Decreasing errors demonstrate that the numerical solutions calculated over the entire soil column and the entire annual period uniformly converge in the analytical solution with respect to both the grid size Δx and the time step Δt. From the convergence of the numerical solutions to the analytical result I can conclude that the thermal model properly handles the heat conduction process with a periodical boundary condition and no phase change.

1.2.2 Benchmark Problem 2: The classical Stefan problem

In this benchmark problem, I consider an infinitely deep fully saturated homogeneous soil column with thermally insulated vertical walls. The soil column is assumed to have a constant porosity η and the phase change occurs at temperature $T = T^*$. The initial temperature of the entire soil column is $T_1 < T^*$. At time $t = 0$ the surface temperature instantly changes to a new constant value $T_2 > T^*$ leading to formation and downward propagation of the phase change boundary. In

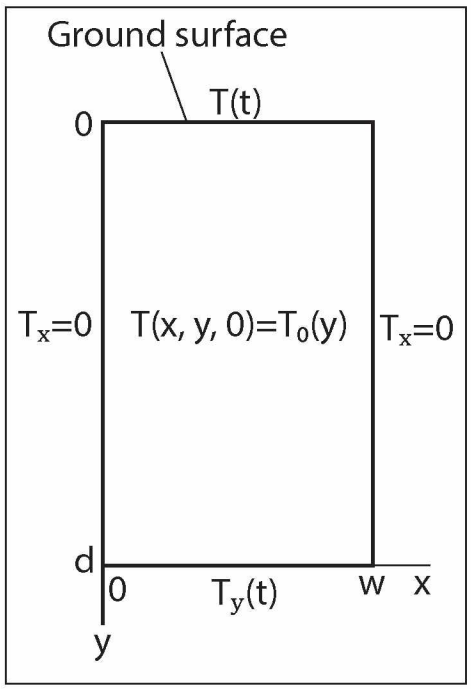

Figure 1.4: A sketch of the computation domain used for Benchmark Problem 1 with the assumed boundary conditions.

this case (often referred to as the Stefan problem) a position of the phase front and temperature dynamics at any point in the soil column can be resolved analytically for any instant of time (*Gupta*, 2003).

To validate my numerical scheme I simulate the thawing of a d = 30 m deep soil column as shown in Figure 1.5. In my numerical experiment at the upper boundary of the column I set a constant temperature T_2, while at the bottom of the soil column, similar to the previous benchmark problem, I set a temperature gradient derived from the analytical solution for this problem. The initial temperature T_1 across the entire column is set to $-1°$C and a new constant surface temperature is $T_2 = 0.5°$C. The phase change occurs at temperature $T^* = -0.001°$C. Zero heat fluxes are prescribed at lateral sides of the column. Thermal properties of the entire column are: $\lambda_s = 1.5$ W/(m $\cdot$ K), $C_s = 2 \cdot 10^6$ J/(m^3 $\cdot$ K), $\eta = 0.3$, where λ_s, C_s stand for the thermal conductivity and the volumetric heat capacity of the soil skeleton and η stands for the ground porosity respectively. Values for bulk thermal conductivity and thermal heat capacity for the ground at different temperatures follow from formulas (1.2) and (1.3). The analytical volumetric unfrozen water content and its numerical implementation are shown in Figure 1.6 by black and red lines, respectively.

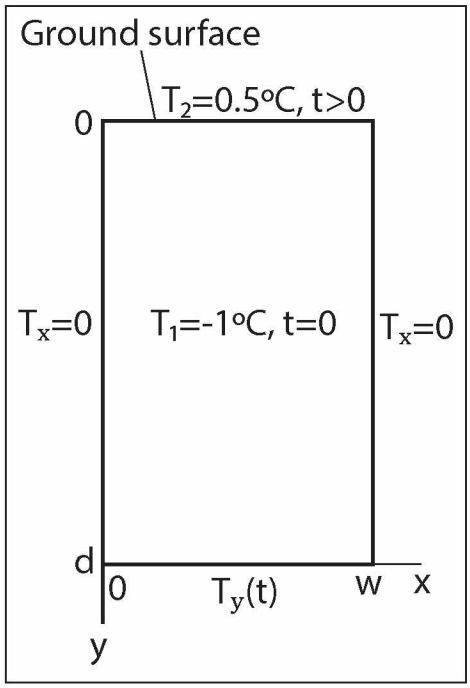

Figure 1.5: A sketch of the computation domain and the boundary conditions for Benchmark Problem 2.

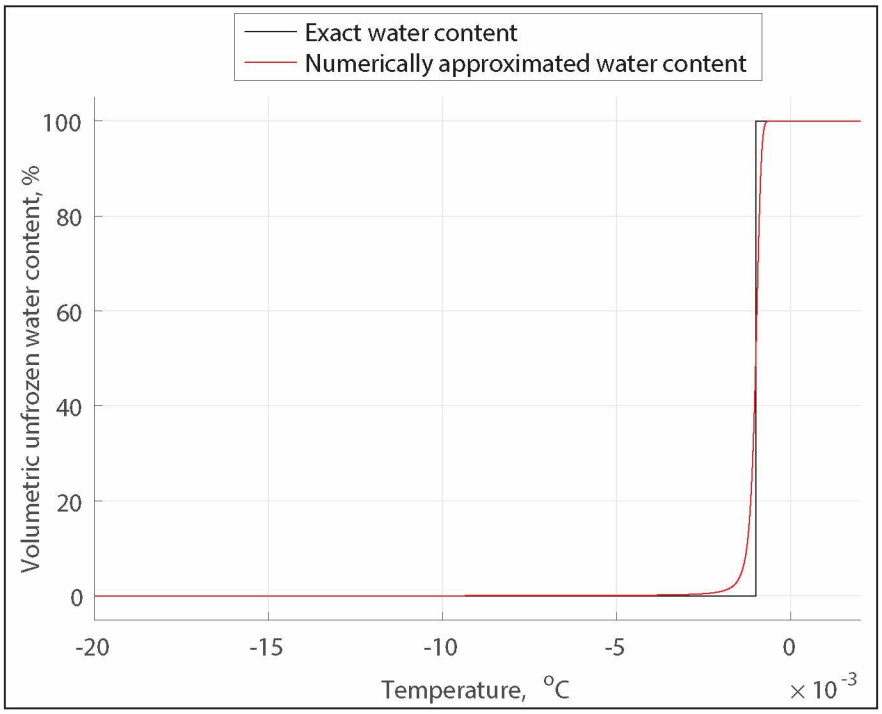

Figure 1.6: Graphs of the exact (black) and the approximated (red) volumetric unfrozen water content parametrization for the soil column.

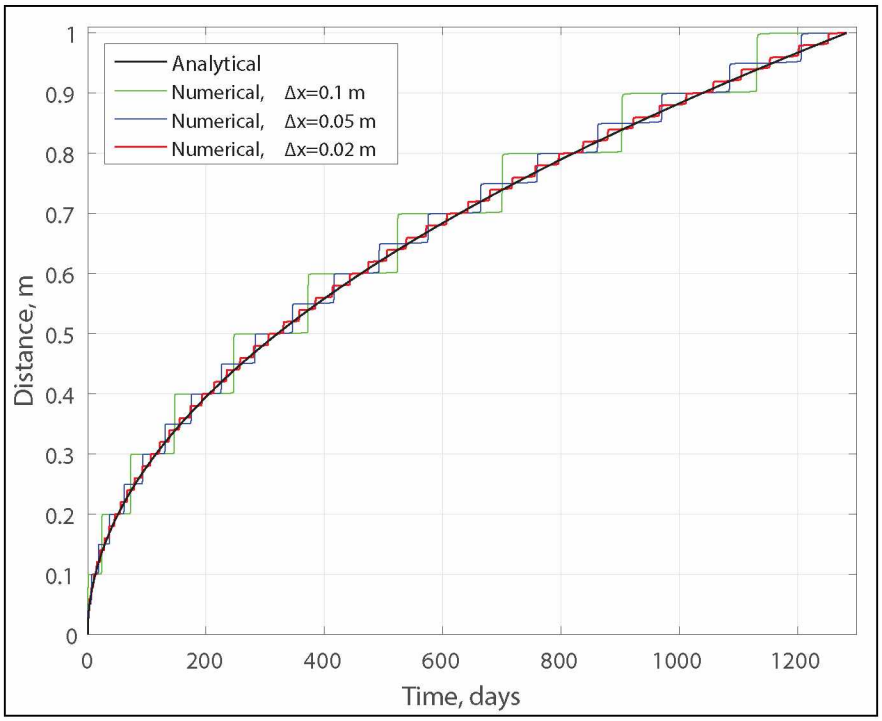

Figure 1.7: Comparison of analytical and numerical solutions for the phase front location.

In the computer experiment I conducted simulations over three different grids. The maximal depth of the simulated thawing is 1 m, and the process of thawing down to this depth takes approximately 1280 days. For each grid soil particles located between ground surface and 1 m are represented by uniform partitions with grid sizes $\Delta x = 0.02,\ 0.05$, and 0.1 m respectively. Again, for simplicity I assume that the width of the computational domain w is equal to Δx. For the depths greater than 1 m grid sizes for each grid gradually increase up to 0.5 m. For each grid the simulations were handled with different maximal time steps $\Delta t = 1,\ 4,\ 16$, and 64 hours.

Comparisons of different solutions show that discrepancies between numerical and analytical results for the phase front location do not significantly depend on a choice of the time step Δt. However, they significantly depend on a choice of the grid size Δx. For this reason I present numerical solutions for the phase front location for different grid sizes Δx and a fixed time step $\Delta t = 1$ hr. A comparative plot of numerical solutions and the exact solution for the phase front location is presented in Figure 1.7. The plot demonstrates that the numerical solutions for the phase front position tend both to over-predict and under-predict its exact location. However, with a reduction of the grid size both over- and under-predictions decrease demonstrating an obvious convergence of numerical results for the phase front position with respect to Δx to a result predicted by exact solution.

Table 1.2: Mean quadratic errors for temperature dynamics for the Stefan problem for different values of Δx and Δt. The errors are presented in 10^{-6} K.

	$\Delta x = 0.1$ m	$\Delta x = 0.05$ m	$\Delta x = 0.02$ m
$\Delta t = 64$ hr	3.615	0.999	0.256
$\Delta t = 16$ hr	3.506	0.865	0.207
$\Delta t = 4$ hr	3.573	0.840	0.182
$\Delta t = 1$ hr	3.626	0.847	0.176

An error analysis for temperature dynamics over the entire soil column was also conducted and results are listed in Table 1.2. Each value in the table represents a mean quadratic temperature error estimated over the entire soil column and the entire time of the simulated process. Note that similar to the case with the phase front the error does not significantly depend on a choice of a time step. Moreover, the discrepancy seems to converge to a non-zero value with respect to Δt for some fixed values of Δx. This behavior could be explained by systematic errors introduced by spatial discretization. On the other hand the error dynamics show a strong decreasing trend with a decrease of the grid size Δx so that a slight increase of errors with a decrease of Δt does not significantly affect this decreasing trend. It allows me to conclude that with a decrease of both Δt and Δx numerical solutions for temperature dynamics converge to the exact solution. The convergence of the numerical results for both temperature dynamics and the phase front to the results predicted analytically allows me to conclude that the thermal model properly handles the process of heat conduction with phase change.

I successfully solved heat equation (1.1) over a 2-D spatial domain for both benchmark problems: the temperature waves problem and the Stefan problem. Solving these problems I successfully validated the proposed model against the process of heat conduction with seasonal freezing and thawing of the ground and boundary conditions including a periodic and a non-periodic temperature variation at the upper surface, and a heat flux at the lower surface. All these conditions are typical for the upper several meters of the ground located in the zone of permafrost. Given a good comparison of numerical and analytical solutions, I assume that the developed model could be applied for simulation of temperature dynamics in a 2-D cross-section of the ground subjected to freezing and thawing and containing permafrost.

1.3 Modeling temperature dynamics across the ice-wedge polygon in Barrow, Alaska

In this section I consider an application of the thermal model for simulation of temperature dynamics in a cross-section of an ice wedge polygon located near Barrow, Alaska. The study site is located at $71°17'$ N $156°36'$ W and is characterized by the presence of high-centered polygons with about

40 cm deep troughs. Aerial photographs of the site are represented in Figure 1.1a. Figure 1.8 also shows positions of snow and temperature sensors at the study site; temperature sensors are located at center, rim, edge and trough of the polygon. At each shallow borehole 16 sensors are installed up to the depth of 1.5 m below the ground surface. In addition to the air temperature sensor, snow depth sensors are installed at center and at one of the troughs of the polygon. Additionally a deep borehole with temperature sensors is located near the study site. Annual measurements in this borehole are available for the depths between 15 and 50 m.

Figure 1.8 illustrates that the temperature shallow boreholes for center, rim, edge and trough are located almost along a straight line, and an approximate geometry of the ground surface along the cross-section is displayed in Figure 1.9. The ground surface is approximated by fitting a spline through elevations of boreholes tops. For parametrization of ground properties I made assumptions about the geometry of the ice wedge and about the properties of the ground along the entire cross-section of the polygon. The hypothetical geometry of the ice wedge approximated by an isosceles triangle is displayed in Figure 1.10a. Soil stratigraphy under the polygon is determined from a core taken at the center of the polygon. Ground properties at the center of the polygon are approximated by several homogeneous ground layers corresponding to each type of soil identified in the stratigraphy. Hypothetical properties of the ground along the entire wedge cross-section are obtained by extrapolation of ground layers identified at the center of the polygon. These layers are assumed to be homogeneous and parallel to the ground surface. The sketch of their geometry is shown in Figure 1.10b. Initial approximations to thermal properties of ground layers are based on results published in (*Nicolsky et al.*, 2007a). Thermal properties of snow are assumed to be constant and uniform through all winter seasons and their initial approximation is based on results published in (*Smith*, 1975). Thickness of snow cover is estimated from sensors located at the center of the polygon and at one of the troughs. Thermal properties of the ice wedge are assumed as the same as thermal properties of pure ice (*de K. Leffingwell*, 1915).

Simulation of ground temperature dynamics over the polygon cross-section is accomplished as follows: Temperature at the upper boundary of the domain is interpolated from hourly air temperature measurements averaged over the 24 hour period for time between September 9, 2012 and October 5, 2014. The lower boundary condition at 30 m depth is assigned in the form of a vertical temperature gradient -0.017 K/m, estimated from deep borehole measurements. Zero temperature gradients based on assumptions about symmetry are established through lateral sides of the polygon cross-section. Initial temperature values at the entire ground cross-section are obtained through a linear interpolation of sensor temperature measurements made on September 9, 2012, an initial date of simulation.

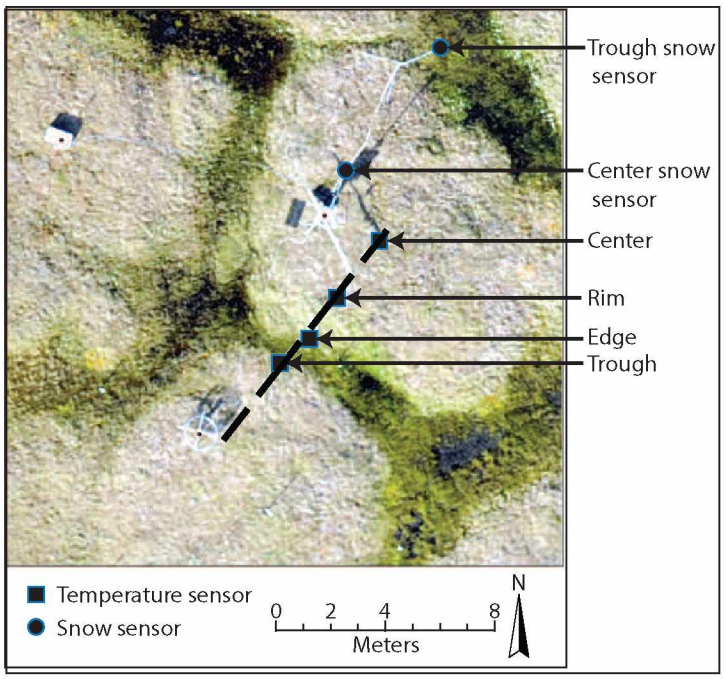

Figure 1.8: An aerial photo of the study area with positions of temperature and snow depth sensors.

Table 1.3: Thermal properties of ground layers calibrated at the center of the polygon.

Depth, m	Ground material	λ_s, $\frac{\text{W}}{\text{m}\cdot\text{K}}$	C_s, $\frac{\text{MJ}}{\text{m}^3\cdot\text{K}}$	η, $\frac{\text{m}^3}{\text{m}^3}$	b	T^*,°C	α
$-0.35-0$	Snow	0.18	0.6	0	–	–	–
$0-0.04$	Live moss	0.643	1.4	0.5	0.33	-0.0001	0.001
$0.04-0.07$	Dead moss	0.67	1.5	0.55	0.33	-0.0001	0.001
$0.07-0.3$	Mineral 1	1.74	2	0.55	0.4	-0.025	0.0022
$0.3-0.49$	Mineral/Organic	0.692	1.75	0.6	0.35	-0.0026	0.001
$0.49-30$	Mineral 2	0.966	2	0.6	0.3	-0.03	0.01
$0.4-15$	Wedge ice	–	–	1	0.999	-0.0001	0.001

Once the boundary and the initial conditions are defined, to calibrate thermal properties of snow and ground layers, I solve a series of heat conduction problems over a soil column at the center of the polygon. Varying thermal properties of snow and ground, I minimize the discrepancy between simulated and measured ground temperatures for the center of the polygon. Calibrated thermal properties for snow and ground layers are listed in Table 1.3. Then I extrapolate the calibrated properties to the entire cross-section and using these properties I calculate temperature dynamics across the entire cross-section of the polygon. The scheme of extrapolation of the ground thermal properties is shown in Figure 1.10b.

Applying the developed numerical model, I compute the soil temperature dynamics and compare the simulated ground temperature dynamics to observations at the center, rim, edge and trough

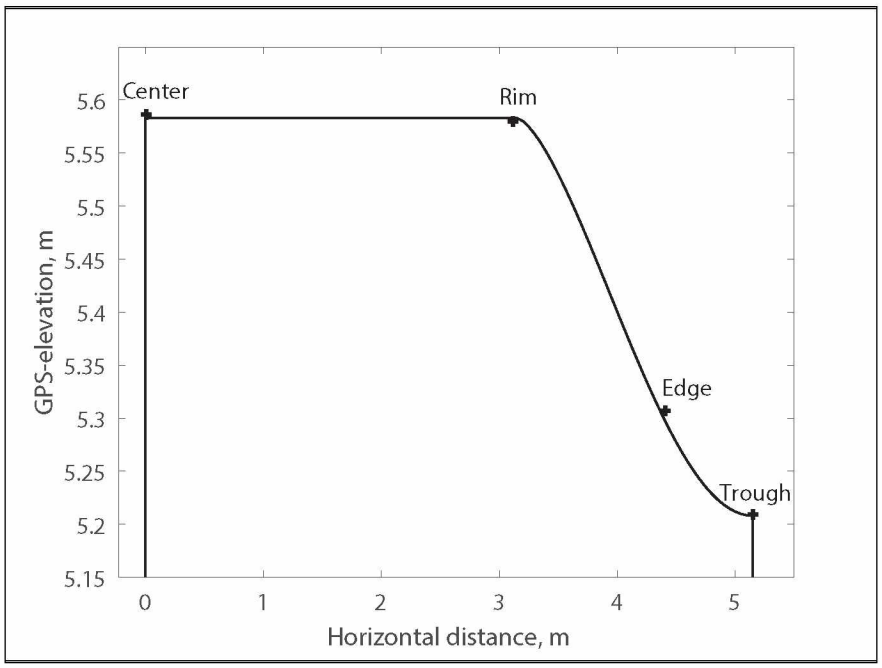

Figure 1.9: Positions of tops of temperature sensor boreholes (black dots) across the cross-section. The line represents a spline fit to the ground surface across the cross-section.

of the polygon in Figure 1.11. The plots are organized in column-wise order, such that plots associated with the same location are all grouped in the same column. The top plots in each column are associated with 0.05 m depth, while plots in the second and third rows are related to 0.5 and 1.5 m depths, respectively. Modeled ground temperature is shown by the red line, while observations are plotted by the black line.

The comparison of the model predictions to its measured counterparts generally shows a good agreement, i.e. the amplitude of annual variations and a timing of freezing are well captured for all locations. The latter is important since the model was forced only with the air temperature and uniform properties for the snowpack layer. For the first winter, 2012-13, we notice that the best match at the 0.05 m depth between the predictions and observations is obtained at the edge of the polygon (Figure 1.11g). A good agreement for the 2012-13 winter is also obtained at the center and rim locations (Figures 1.11b and 1.11g). However, the model shows a positive bias with respect to observations at the trough for the same time period (Figure 1.11h). The positive bias propagates deeper and modeled temperatures are about $1°C$ higher than the corresponding observations at the 1.5 m depth (Figures 1.11e, 1.11f, 1.11k and 1.11l). A possible cause of this bias lies primarily in the oversimplified parametrization of the snowpack and to some degree is related to discrepancies in the initial ground temperature parametrization, air temperature forcing and the prescribed properties of the ground material. However, upon further investigation, I notice

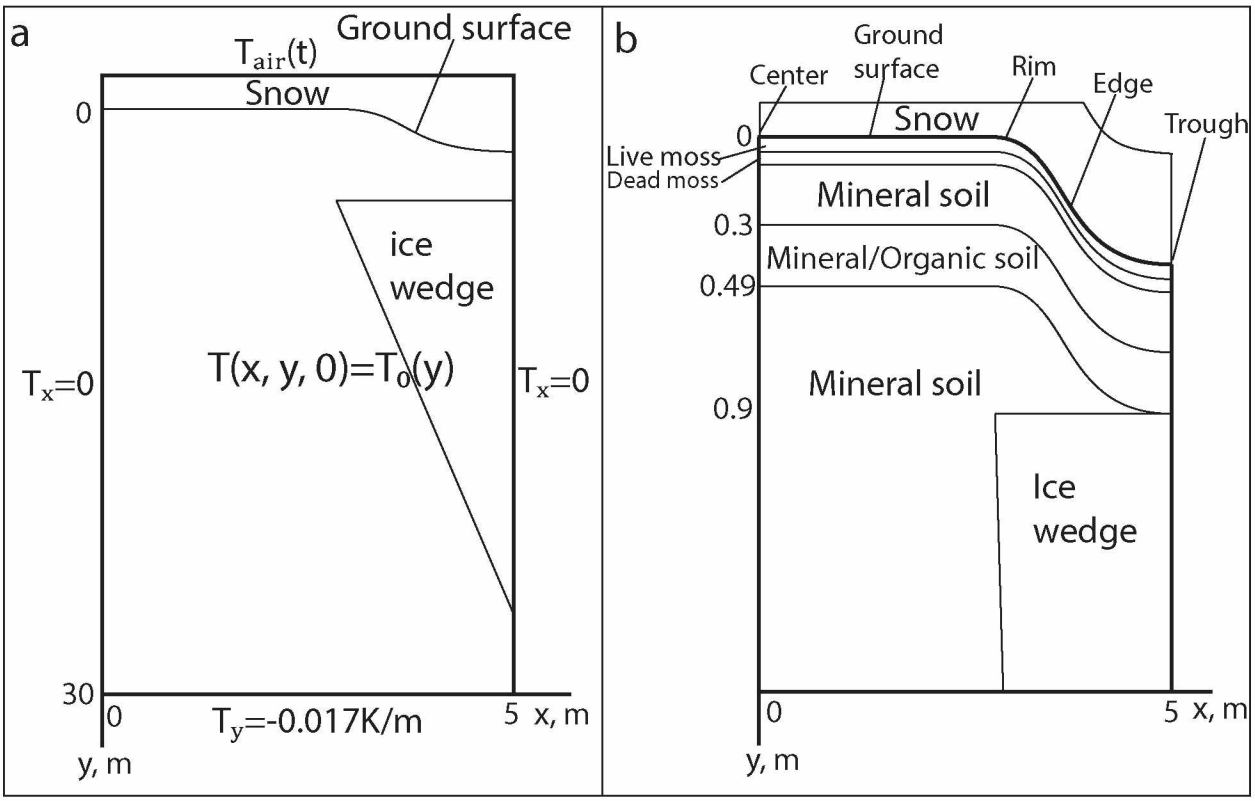

Figure 1.10: a) A sketch of the hypothetical geometry of the ice wedge and initial and boundary conditions for the numerical experiments. b) A scheme of ground layers at the 2-D cross-section around the ice wedge.

that the positive bias in the modeled ground temperature disappears during the 2013-14 winter and numerical calculations match the observations very well.

As it was observed in many other previous studies (*Zhang et al.*, 2001; *Nicolsky et al.*, 2007b, 2009; *Jafarov et al.*, 2013), the model underestimates the observations in the spring; the difference could be as much as 5°C. A reader is prompted to examine disparity between the modeled and observed temperatures in the late May - early June periods. Another disparity between the modeling results and the observations occurs when the ground starts to freeze and a 0°C curtain appears. It looks like the ground material in the trough proceeds through the phase change process in the numerical experiment sooner than it does in reality. This discrepancy is likely attributed to the high water content in the trough and associated with it a significant sink of the latent heat. An early snow accumulation in the trough and hence additional snow insulation effects might also contribute to the delay in onset of freezing. I will discuss implications of the increased water content to the ground temperature dynamics in the trough later in this chapter.

To further analyze results of the numerical experiments, I plot snapshots of the modeled and observed (linearly interpolated between the temperature sensors) temperatures at several moments of time in Figure 1.12. In particular, Figures 1.12a-i present the process of autumn-winter ground freezing and Figures 1.12j-r present the process of spring-summer ground thawing. The first column corresponds to the observations, while the second one is related to numerical computations. The third column is related to the numerical experiment in which the water content is assumed to be higher near the trough. All figures share the same color code and the time stamp is shown at the title of each plot.

I notice that the modeling results compare well with the observations in September (Figures 1.12a and 1.12b) through November (Figures 1.12d and 1.12e). However, in early December, the observations show that the ground material underneath the trough is slightly below freezing (Figure 1.12g), while the ground material in the numerical experiment (Figure 1.12h) is significantly colder. As mentioned earlier this disparity could be explained by the snow accumulation and increased water content in the trough. Therefore, I consider another numerical experiment with the higher water content in the trough. For this purpose we increase the soil porosity of the ground material above the ice wedge, within 1.5 m from the center of the ice wedge. As mentioned earlier, numerical results for this numerical experiment are shown in the third column in Figure 1.12. The most significant difference between the two numerical experiments (uniform properties vs. increased in the trough) is attained for the month of December 2012. I note that the modeled ground temperature in the additional numerical experiment (Figure 1.12i) very well captures the observations (Figure 1.12g); the spatial distribution of the modeled ground temperature reproduces the shape of the

warm bulge observed underneath the trough.

I also supplement time series plots in Figures 1.11h-l with results of the additional numerical experiment. Since, the water content is only increased near the trough area, differences between the modeled ground temperature dynamics, between the two models, at the rim and center are not significant and are thus omitted. I enlarged plots related to the temperature dynamics in the trough during fall-winter 2012 in Figure 1.13. The increased areas are indicated by dashed lines in Figures 1.11h and 1.11j. I would like to emphasize that the increased water content near the trough results in the delayed onset of freezing and a better match with observations.

Another significant difference between the modeled and observed ground temperatures is noticed during the snow melt period in late May through the middle of June. A reader may inspect Figures 1.12j, 1.12k as well as Figures 1.12m, 1.12n and find a significant difference between observed and predicted ground temperatures for May 25 and June 10, 2013. These discrepancies are related to much warmer ground surface temperatures in the trough. The spring snowmelt waters might accumulate in depressions, such as troughs, and increase the ground temperature to 0°C. On the other hand, since the snowmelt period lasts in the Barrow area only two or three weeks, discrepancies in the modeled temperature dynamics are limited to the upper part of the active layer and do not significantly affect the results for temperature dynamics for the rest of the year. A good agreement between results on August 10, 2013 is obtained, as shown in Figures 1.12p-r.

1.4 Limitations

In this research I apply the numerical model to simulate temperature dynamics in the 2-D cross-section of the ice wedge polygon. First, I estimate the thermal properties of the ground material at the center of the polygon and then extrapolate the recovered properties across the polygon. Finally, I simulate temperature dynamics at the entire cross-section. There are some inherent uncertainties in the proposed approach and in the rest of this section, I describe some potential shortcomings.

To justify my simulations for the center of the polygon I assume that the soil is fully saturated and processes such as water migration, frost heave and thaw settlement could be considered negligibly small. Also I do not consider an effect of snowmelt on a heat transfer process and I rely on approximation of the snow thermal properties by constant values. By extrapolating thermal properties for the rest of the cross-section I additionally assumed that an ice wedge geometry is well-approximated by an isosceles triangle, as shown in (*Pewe*, 1963) Figure 1 with a flat top and the thermal properties of the ground and snow at the cross-section are well-approximated by homogeneous parallel layers (see Figure 1.10b). In nature, ice wedges have rather arbitrary shapes, however the developed model could be easily modified to accomodate these irregularities.

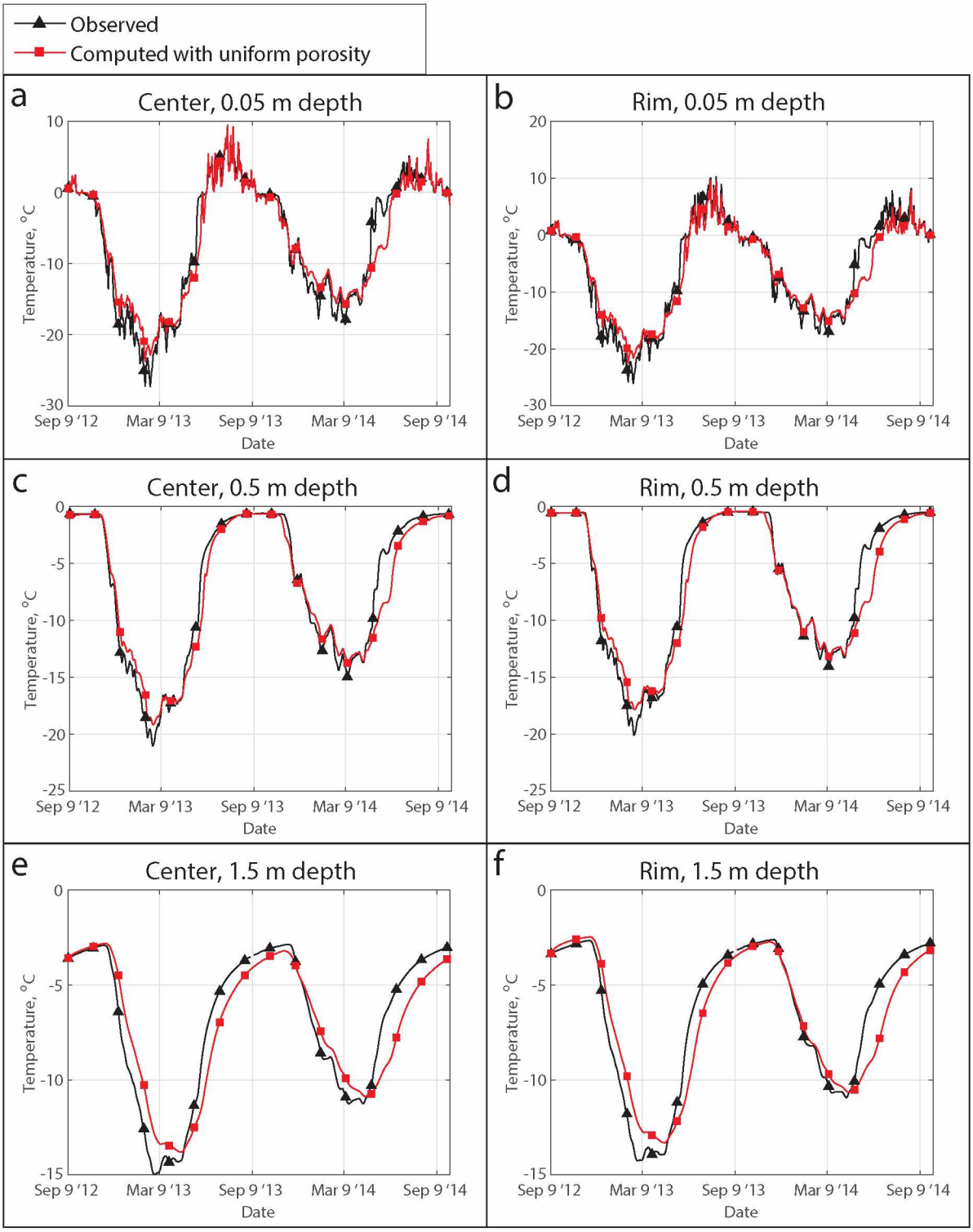

Figure 1.11: Comparison of observed (black) and computed ground temperature dynamics for the uniform porosity (red). Left and right panels show results under the center of the polygon and the under the polygon rim, respectively.

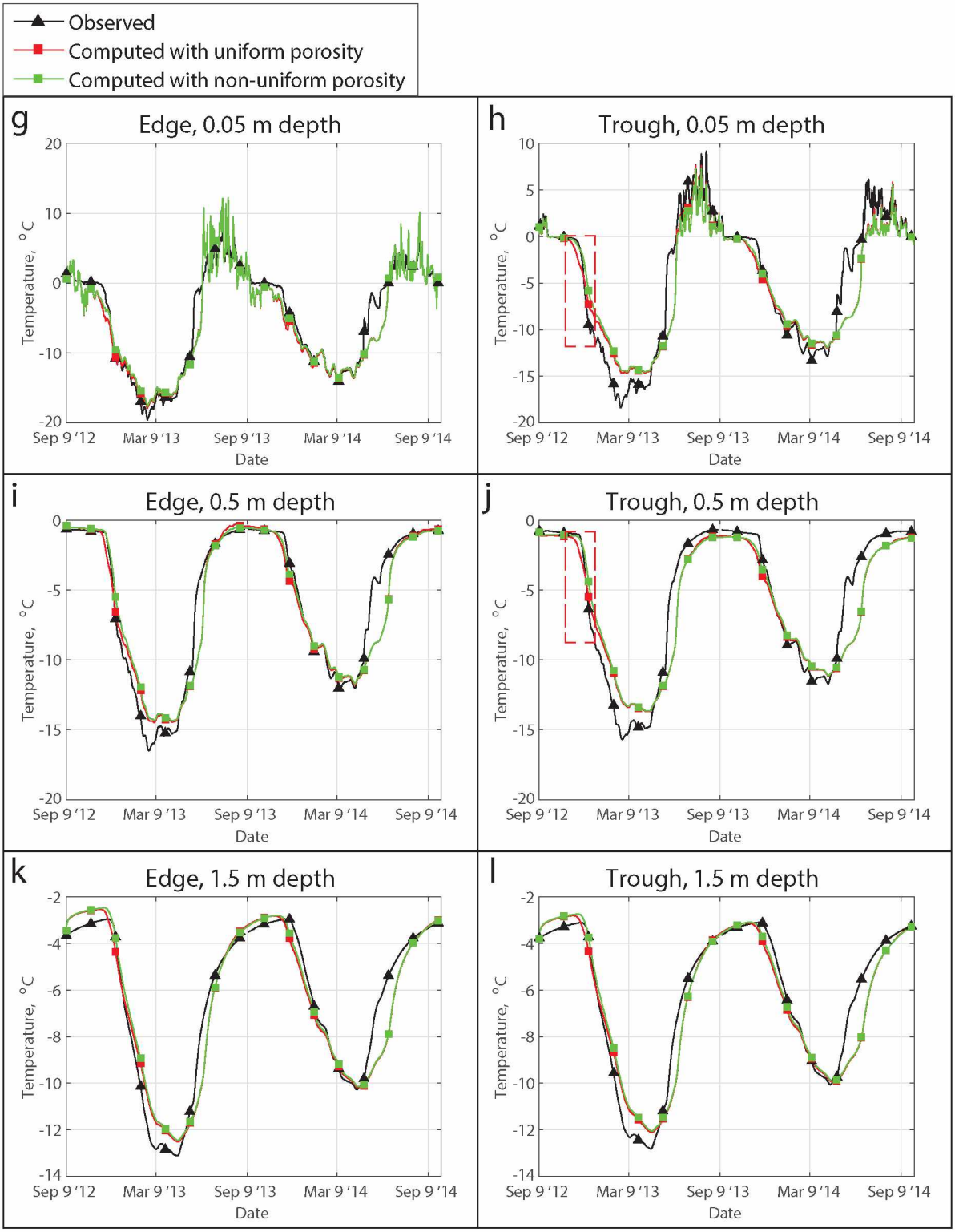

Figure 1.11: continued. Comparison of observed (black) and computed ground temperature dynamics for the uniform porosity (red) and the increased porosity (green) in the trough. Left and right panels show results under the edge of the polygon and under the trough, respectively. The areas on panels h and j marked by red dashed rectangles are shown enlarged in Figure 1.13.

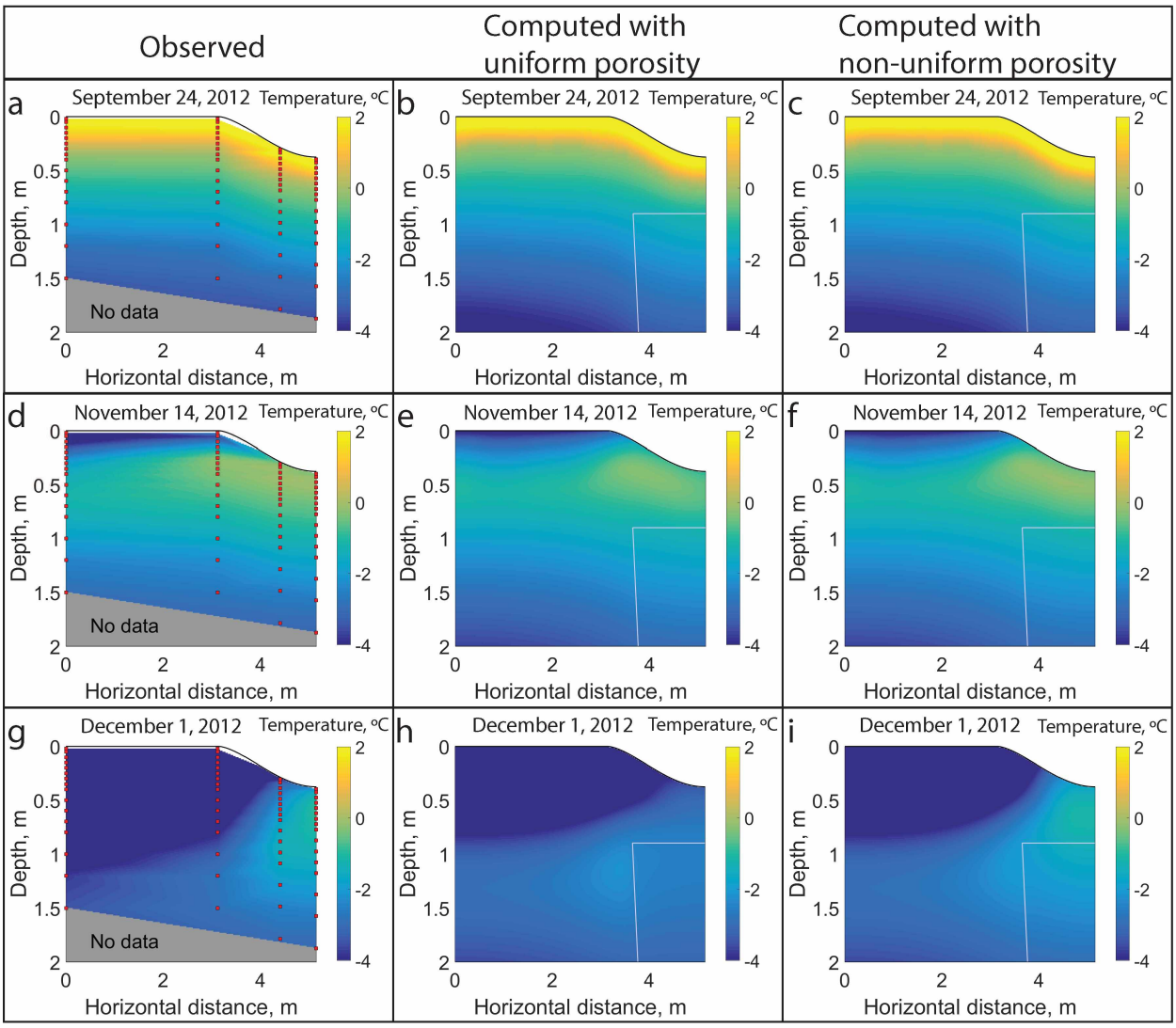

Figure 1.12: Comparison of computed with non-uniform porosity, observed and computed with uniform porosity temperatures at the ground cross-section for September 24 (a, b and c), November 14 (d, e and f), and December 1, 2012 (g, h and i). Red squares in left panels show locations of temperature sensors in the ground.

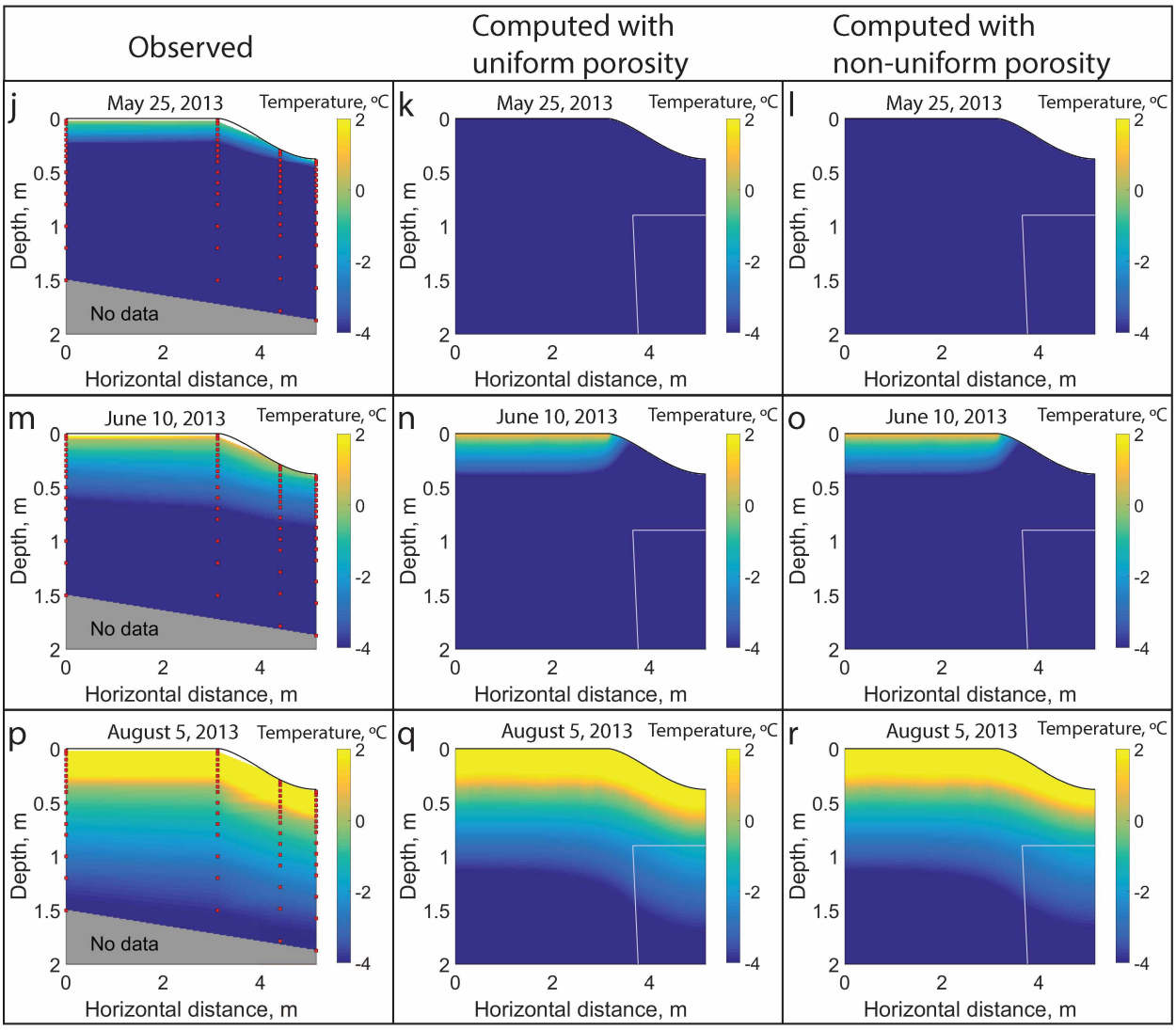

Figure 1.12: continued. Comparison of computed with non-uniform porosity, observed and computed with uniform porosity temperatures at the ground cross-section for May 25 (j, k and l), June 10 (m, n and o), and August 5, 2013 (p, q and r). Red squares at the left column show locations of temperature sensors. Red squares in left panels show locations of temperature sensors in the ground.

I approximate ground properties for the entire cross-section by parallel layers (organic material, mineral material) parallel to the ground surface such that the thermal properties and the water content are homogeneously distributed within each layer. At the same time, several factors can affect the composition and layering of the ground material. The layer geometry can be disturbed by upturning, due to summer expansion of permafrost around a growing ice wedge (*Lachenbruch*, 1963), subsidence due to previous melting of an ice wedge and erosion of the polygon. The top of the ice wedge might have severe irregularities and may not be flat, as assumed in the model. The thermal properties of ground material are also likely to be affected by cryoturbation processes over the long term interval (*Bockheim and Hinkel*, 2004). The presence of a mineral/organic soil layer between two layers of silt under the center of the polygon (see Figure 1.10b) points to the likelihood of the cryoturbation process in Barrow. Moreover, because of the elevation gradient at the polygon, water may drain into natural depressions corresponding to troughs (*Liljedahl et al.*, 2012) and thus it is reasonable to expect that the water content in the trough area is to be greater than that in the rest of the polygon. Additionally I note that the aerial photo depicted in Figure 1.8 illustrates that the trough area is more vegetated than the rest of the polygon. Because of the more developed vegetation, possibly a higher water content is expected in the upper organic layers around the trough. Therefore, the thickness and the thermal properties of the organic layers in the trough might be different from those related to the elevated part of the polygon.

I see at least two approaches to further enhance the agreement between predicted and observed temperature profiles. First, it is possible to analyse soil samples and then to calibrate ground water contents and thermal properties at each borehole separately. Then, applying interpolation techniques it is possible to define these properties for the entire cross-section. This improvement would hypothetically allow me to improve the quality of prediction for temperature dynamics at the entire cross-section. Second, it is possible to define thermal properties of snow and values of porosities for upper ground layers as time dependent and change their values at different seasons. This approach can improve an agreement between observed and computed temperatures at the ground surface and in particular for the snowmelt period, at which the agreement is rather poor.

With all simplifications regarding the water content, thermal properties of the ground material and snowpack, as well as the geometry of layers, a good agreement between observed and simulated temperature dynamics was obtained. I think that there are other possibilities to reduce the discrepancy between simulations and observations without change of the numerical model. In particular improving parametrization of water content in the trough I was able to reduce the discrepancy for the period of winter freezing. Future steps may include improving snow accumulation and melt processes. In particular, the thermal properties of snow may vary throughout the season due to

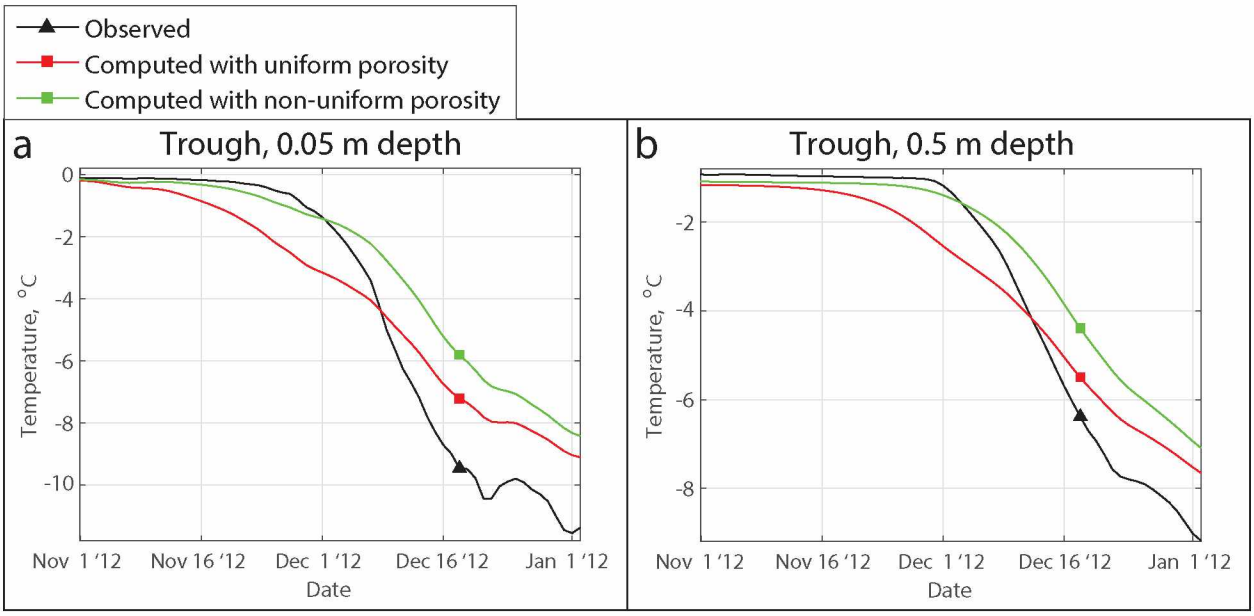

Figure 1.13: Panels a and b show enlarged areas marked by red dashed rectangles on Figures 1.11h and 1.11j respectively. These areas present calculated and observed temperature dynamics under the trough for the period of seasonal ground freezing at fall-winter 2012.

snow compaction (*Côté et al.*, 2012), exposure to wind, temperature gradients, and melt. The process of phase change in snow leads to an increase of its apparent heat capacity. Produced water percolates down to the ground bringing latent heat to the frozen soil.

Chapter 2

Simulation of ice wedge degradation

2.1 Description of a mechanical model of ground subsidence coupled with the model for temperature dynamics around an ice wedge

In this section I describe my approach for modeling processes of ice wedge degradation and trough formation. The process of melting of the ice wedge is simulated through heat equation (1.1), assuming that heat conduction is a dominant heat transfer process in the ground, snow and ice. To simulate the process of trough formation I assume that the ground presses on water produced by the melting ice wedge, water drains through cracks and triggers ground subsidence. I assume that the subsidence is mostly controlled by deformation properties of the ground and these properties can have a significant effect on formation of small troughs above melting wedges. Following these assumptions I describe soil behavior with a rheological model.

2.1.1 Mechanical problem

Before I introduce a mechanical model for soil deformation, I would like to review some mechanical models used to describe this process. One of the simplest models describing the soil deformation is the poroelastic model. It was employed by *Gambolati et al.* (2001) for numerical analysis of land subsidence above depleted reservoirs; by *Qi et al.* (2012), *Wang et al.* (2015b) and by *Yao et al.* (2012) for the analysis of soil thaw consolidation. Applicability of the visco-elastic Maxwell model for parametrization of behavior of soils undergoing compression deformations was considered by *Zolotarevskaya* (2003). A visco-elasto-plastic constitutive relationship was employed by *Luo and Feng* (2011) for numerical modeling of the ground subsidence due to groundwater exploitation. The elasto-plastic Drucker-Prager model (*Drucker and Prager*, 1952) and a combination of the visco-elastic Maxwell, Kelvin-Voigt models and the visco-plastic Bingham model (*Bingham*, 1916) were employed by *Wang et al.* (2013). In particular, the Drucker-Prager model (*Drucker and Prager*, 1952) was used by *Wang et al.* (2013) to simulate soil thaw consolidation, and the combination of other models was employed to model creep of frozen soil. As soil models become more complicated and describe the time-dependent behavior of soil associated with applying and removing large loads, they include elastic, viscous and plastic components into their constitutive relationships.

Here I would like to point out that in my simulated process I have no external loads applied to the ground and the only loads the ground undergoes are due to its own weight. These loads are assumed to be sufficiently small so that the ground deformation under these loads could be described by a linear elastic relationship. Because of the bonds existing between soil particles, a

time delay between melt of ground ice and an elastic response of the ground is possible. I assume that I can effectively parameterize this delay by introducing a linear viscous component into my rheological model. Another effect controlling the trough formation, is drainage of water appearing from melted wedge ice. For example, for low-permeable clay soils this effect can be significant. *Lewis et al.* (2012); *Yao et al.* (2012); *Qi et al.* (2012); *Wang et al.* (2015a,b) parameterized the water drainage by Darcy's law. However, these papers were focused on the cases where the excess water was well-mixed with soil grains. In my case, the ground is assumed to subside into a water body, as shown in Figure 2.1. Also, because of cracks in the ground I assume that water drains instantly under the pressure of ground layers and therefore the effect of melt water on ground subsidence is negligibly small.

Based on these assumptions I chose to parameterize the ground deformation above a melting ice wedge by the linear visco-elastic Kelvin-Voigt model. According to (*Eringen*, 1980) the stress-strain relationship for a linear Kelvin-Voigt isotropic material can be defined as

$$\boldsymbol{\sigma} = \lambda_e tr(\boldsymbol{\epsilon})\mathbf{I} + 2\mu_e\boldsymbol{\epsilon} + \lambda_v tr\left(\frac{\partial\boldsymbol{\epsilon}}{\partial t}\right)\mathbf{I} + 2\mu_v\frac{\partial\boldsymbol{\epsilon}}{\partial t} \tag{2.1}$$

$$\boldsymbol{\epsilon} = \frac{1}{2}(\nabla\mathbf{u} + (\nabla\mathbf{u})^*) \tag{2.2}$$

where

$\mathbf{u} = \mathbf{u}(\overline{\mathbf{x}}, t) = [u_x, u_y, u_z]$ [m] is the soil displacement

$\overline{\mathbf{x}} = (x, y, z)$ [m] is the 3-D coordinate describing a position in space

t [s] is time

$\boldsymbol{\epsilon} = \boldsymbol{\epsilon}(\overline{\mathbf{x}}, t) = \begin{bmatrix} \epsilon_{xx} & \epsilon_{xy} & \epsilon_{xz} \\ \epsilon_{xy} & \epsilon_{yy} & \epsilon_{yz} \\ \epsilon_{xz} & \epsilon_{yz} & \epsilon_{zz} \end{bmatrix}$ $[m/m]$ is the 3×3 second order strain tensor

$\mathbf{I}$ is the 3×3 second order identity tensor

$\boldsymbol{\sigma} = \boldsymbol{\sigma}(T, \overline{\mathbf{x}}) = \begin{bmatrix} \sigma_{xx} & \sigma_{xy} & \sigma_{xz} \\ \sigma_{xy} & \sigma_{yy} & \sigma_{yz} \\ \sigma_{xz} & \sigma_{yz} & \sigma_{zz} \end{bmatrix}$ $[Pa]$ is the 3×3 second order effective stress tensor

$\lambda_e = \lambda_e(T, \overline{\mathbf{x}})$ $[Pa]$ and $\mu_e = \mu_e(T, \overline{\mathbf{x}})$ $[Pa]$ are Lame elastic modula

$\lambda_v = \lambda_v(T, \overline{\mathbf{x}})$ $[Pa \cdot s]$ and $\mu_v = \mu_v(T, \overline{\mathbf{x}})$ $[Pa \cdot s]$ are viscous modula

$T = T(\mathbf{x}, t)$ $[K]$ is the temperature and

$\mathbf{x} = (x, y)$ $[m]$ is the 2-D coordinate describing a position in the ground cross-section.

Since mechanical variables are defined for points in 3-D space, I employ a three-dimensional coordinate $\overline{\mathbf{x}}$ to describe mechanical properties of the ground, as well as with a two-dimensional coordinate $\mathbf{x}$ I describe properties related to temperature dynamics in a 2-D ground cross-section.

Following numerous field observations it is reasonable to expect ground deformations to be slow, with creep responses lasting for hours and days. This fact allows me to assume that accelerations for soil particles are also negligibly small and can be approximated by zero. Following these assumptions

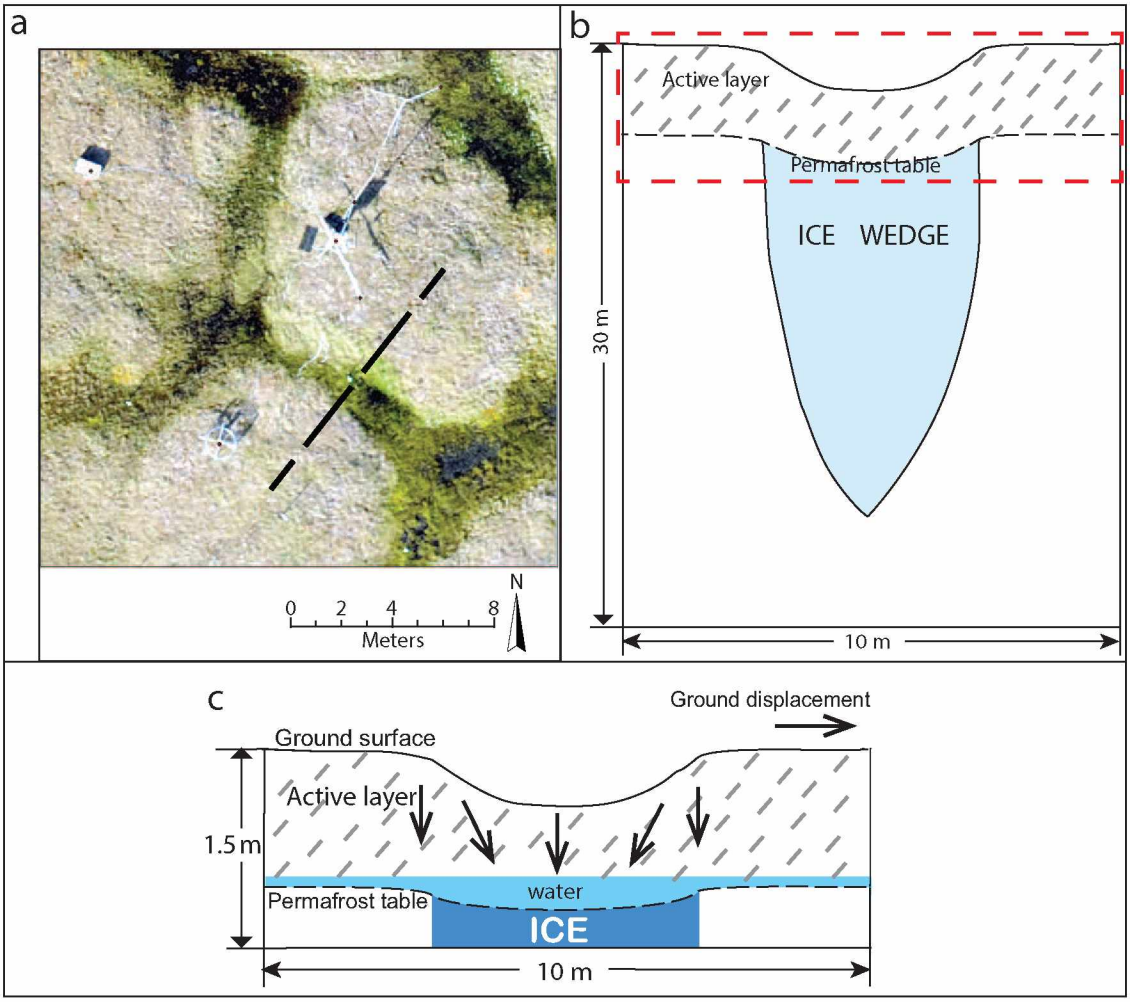

Figure 2.1: (a) A view of high-centered ice wedge polygons near Barrow, Alaska, 71°17′N 156°36′W. The dashed black line shows the surface trace of the cross-section. (b) A schematic sketch of the hypothetical ground cross-section containing an ice wedge. The dashed red line encloses an area presented in plot (c). (c) A scheme of the processes of ice wedge degradation and ground subsidence.

I parameterize a relationship between the effective stress $\boldsymbol{\sigma}$ and the gravity load for the soil by Cauchy's equation of equilibrium (*Holzapfel*, 2000):

$$\nabla \cdot \boldsymbol{\sigma} + \rho \mathbf{g} = \nabla p \tag{2.3}$$

where p $[Pa]$ is the pore water pressure, $\mathbf{g} = [0, 9.8, 0]$ $[m/s^2]$ is the gravity acceleration, ρ $[kg/m^3]$ is the soil/ice density. The ground pore water pressure is parameterized through the equation

$$p = \rho_w |\mathbf{g}| h, \tag{2.4}$$

where $\rho_w = 1000$ kg/m^3 is the density of water, $h = h(\theta_w,\ \overline{\mathbf{x}},\ t)$ $[m]$ is the height of the ground water table above the point $\overline{\mathbf{x}}$, $\theta_w = \theta_w(T, \mathbf{x})$ $[m^3/m^3]$ is the volumetric unfrozen water content.

The system of equations (2.1), (2.2), (2.3) and (2.4) is solved over a domain denoted in Figure 2.2b as $A'B'E'F'$. This domain is a part of a heat equation domain denoted as $ABEF$ which is shown in Figure 2.2a. In Figure 2.2b boundary $B'E'$ represents the ground surface. Lower boundary $A'F'$ represents the ground located at some depth d' exceeding the maximal depth of the active layer in the cross-section. Left boundary $A'B'$ represents the center of an ice wedge polygon. Imposing symmetry assumptions on an ice wedge polygon and on a 2-D ice wedge cross-section discussed in Chapter 1 I assume that no horizontal displacements occur along boundaries $B'E'$ and $E'F'$, so for each point of $B'E'$ and $E'F'$ the condition $u_x = 0$ holds. Zero vertical displacement $u_y = 0$ is prescribed at boundary $A'F'$, assuming that deformations in permafrost are negligible. Next, for most of the observed ice wedges and in particular in the example in Figure 2.1 the ice wedge is much longer in the direction parallel to the contraction plane (z-direction) than in the cross-sectional direction (x-direction). Also, as discussed in Chapter 1, temperature dynamics around an ice wedge do not significantly change along the contraction plane. Then it is reasonable to expect the processes of ice wedge degradation and ground subsidence to be more or less uniform in the longitudinal z-direction. These facts allow me to assume that ground displacements along the contraction plane in z-direction are negligibly small and can be approximated by zero. Following these assumptions I simulate ground deformation in the 2-D cross-section parallel to xy-plane as a plane strain problem prescribing the condition $u_z = 0$ at each point of domain $A'B'E'F'$. Since I impose no external load at the ground surface, I prescribe every component of effective stress $\boldsymbol{\sigma}$ as zero at each point of boundary $B'E'$. An initial displacement $\mathbf{u}_0$ at domain $A'B'E'F'$ for simplicity is also defined as zero, so at the initial instant of time the ground is assumed to be not deformed.

The finite element method (*Zienkiewicz and Taylor*, 1991) with a moving two-dimensional computation grid is employed to the system of equations (2.1), (2.2), (2.3) and (2.4) over 2-D domain

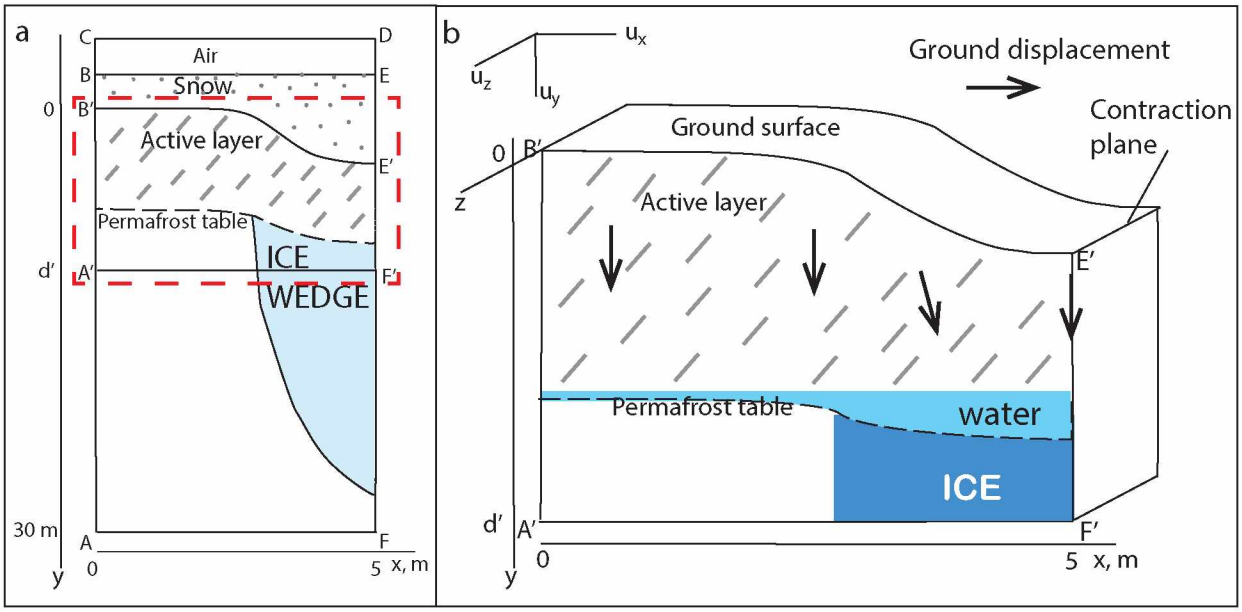

Figure 2.2: (a) A sketch of the domain for simulation of the temperature dynamics and melting of the ice wedge. Red dashed line encloses the area over which the ground displacements are simulated. (b) A sketch of the domain for simulation of the ground deformations above the melting ice wedge.

$A'B'E'F'$. The implicit Euler method is employed to discretize and solve the resultant system with respect to time. At each time step a deformed grid is checked for consistency. If consistency conditions for the grid are not met, the time step is halved and calculations are repeated. To consider both thermal and mechanical problems over ground layers of different depth I divided the entire computational domain on three subdomains. The entire domain is denoted by Ω and the subdomains are denoted by Ω_1, Ω_2 and Ω_3. These subdomains represent a shallow deforming ground layer, a deep ground layer containing only permafrost, and the seasonal snow cover respectively. For each subdomain a separate subgrid is generated and a grid for the whole cross-section Ω is obtained by joining these subgrids together. The grid for entire domain Ω I denote by Γ as subgrids for Ω_1, Ω_2 and Ω_3 I denote by Γ_1, Γ_2 and Γ_3 respectively. A sketch of the domains and the grids is presented in Figure 2.3. Ground deformation is calculated over the subdomain Ω_2 and ground temperature dynamics are calculated over the entire domain Ω.

The process of ground subsidence associated with ice wedge degradation at summer time leads to moving of a boundary between Ω_1 and Ω_3. Consequently, some cells of the subgrid Γ_3 which represents the air during the snowless period get distorted. Distortion of cells for this grid may lead to an inaccurate simulation of temperature dynamics across the snow cover and consequently in the upper layers of the ground. To resolve this issue, retriangulation of the subgrid Γ_3 is done every autumn, between periods of ground subsidence and seasonal snow fall.

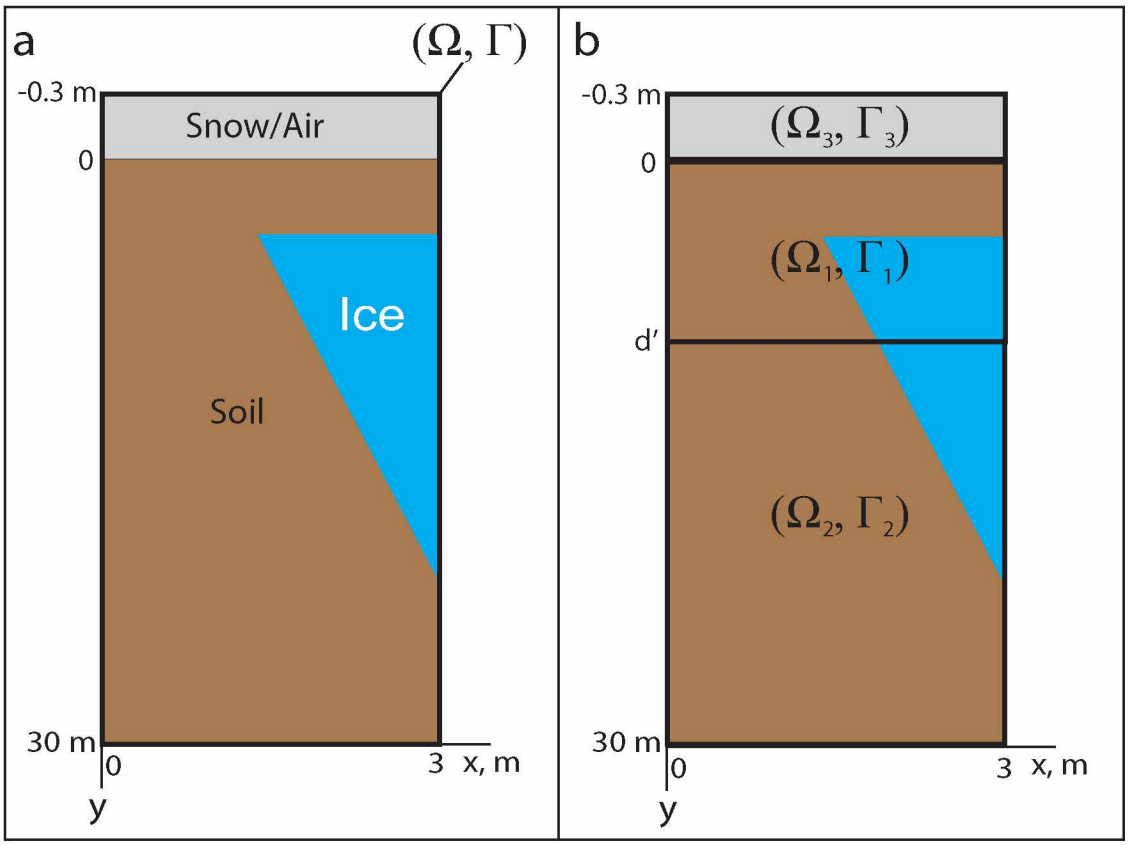

Figure 2.3: A scheme of subdivision for the spatial domain Ω and corresponding grid Γ. (a) A system of entire thermo-mechanical domain Ω and grid Γ. (b) Subdivision of the entire domain/grid Ω/Γ on subdomains/subgrids Ω_i /Γ_i, where $i = 1, .., 3$.

Next, I would like to discuss parametrization approaches employed in my simulations for elastic modulus and viscosity for frozen and thawed ground materials. Many field observations and laboratory experiments show that elastic modula of soil samples increase upon their freezing and decrease when they are thawing. It is reasonable to expect similar changes for their viscosity. An increase of elastic modulus and viscosity of soil with freezing can be explained by the existence of bonds between molecules of ice in soil. With melting of ice these bonds disappear. Also, the ice itself could be treated as a viscoelastic Kelvin-Voigt material with large values for elastic modulus and viscosity. On the other hand water behaves like an inelastic material and has a very small viscosity in comparison with ice. For these reasons for every ground material I introduce a pair of elastic modula, E_{fr} and E_{th} and a pair of viscosity coefficients, μ_{fr} and μ_{th} corresponding to the frozen and thawed state of a ground material respectively.

In the case where a soil sample has both ice and unfrozen water, it is reasonable to expect the sample to have intermediate visco-elastic properties. For this reason I chose to interpolate elastic modulus and viscosity for a partially frozen ground material through its volumetric unfrozen water content $\theta(T)$. According to introduced interpolation mechanical properties for ground materials other than wedge ice are calculated as

$$E(T) = E_{\text{fr}}^{1-\theta(T)/\eta} \cdot E_{\text{th}}^{\theta(T)/\eta} \text{ and } \mu(T) = \mu_{\text{fr}}^{1-\theta(T)/\eta} \cdot \mu_{\text{th}}^{\theta(T)/\eta} \tag{2.5}$$

where T [°C] is the temperature, η $[m^3/m^3]$ is the ground porosity, $\theta(T)$ $[m^3/m^3]$ is the ground volumetric unfrozen water content, indices {fr, th} in this context stand for the properties of frozen and thawed ground material respectively. One can notice that a similar parametrization was introduced by (*de Vries*, 1963) for soil thermal conductivity and was discussed in Chapter 1.

To simulate the process of ground subsidence upon melting of an ice wedge I use different values of elastic modulus and viscosity for ice and water. It is important to notice that because of the large volumetric latent heat for water, melting of ice is associated with a large sink of heat. Consequently a careful approach for simulation of ground subsidence upon melting of ice is required. For this reason I calculate mechanical properties for ice and water as

$$E(T) = \begin{cases} E_{\text{fr}} & \text{if } T < T_* \\ E_{\text{th}} & \text{otherwise} \end{cases} \text{ and } \mu(T) = \begin{cases} \mu_{\text{fr}} & \text{if } T < T_* \\ \mu_{\text{th}} & \text{otherwise} \end{cases} \tag{2.6}$$

where T [°C] is the temperature and T^*, [°C] is the freezing point depression for ice/water, indices {fr, th} stand for the properties of ice and water respectively.

2.1.2 Coupled thermo-mechanical problem

In this subsection I would like to describe my numerical algorithm for a coupled thermo-mechanical problem, in which the process of ice wedge degradation is combined with the process of ground subsidence. Since visco-elastic properties of ground materials are temperature dependent, I need to calculate temperature dynamics of the ground and ice wedge to predict these properties. On the other hand, deformation of the ground also affects the temperature dynamics of the ground and ice. These facts imply that for successful modeling of both ground temperature dynamics and its mechanical behavior at each time step I need to solve both heat equation (1.1) and mechanical equations (2.1), (2.2), (2.3) and (2.4).

There exist different approaches for solving these equations with respect to time. Solving the heat equation and the mechanical system as a fully coupled system looks like the most correct one. However, to implement this approach I would need to introduce advection terms into the heat equation, making the heat equation more complicated. Also handling the advection terms in numerics is associated with additional accuracy issues. Since the coupled system would be non-linear, iterations for the entire system would be needed to solve it by the fully implicit Euler method. These iterations, combined with iterations employed for solving heat equation (1.1) would make the computations very slow.

Here I introduce an alternative approach which I believe would allow me to achieve a reasonable accuracy of the solution with reasonable computational costs. Suppose I calculated ground temperature dynamics $T(t)$ and ground displacements $\mathbf{u}(t)$ at time t and I want to calculate them for time $(t+\Delta t)$, where Δt is the time step. Then first, with temperature dynamics $T(t)$ and boundary conditions for the thermal problem I solve heat equation (1.1) and obtain temperature distribution for the next time step $T(t+\Delta t)$. Second, with a new temperature distribution $T(t+\Delta t)$ I estimate values of elastic modulus $E(T(t+\Delta t))$ and viscosity $\mu(T(t+\Delta t))$ for ground materials and ice. Third, employing mechanical properties at time $(t+\Delta t)$, displacements $\mathbf{u}(t)$ and boundary conditions for the mechanical problem I solve mechanical equations (2.1), (2.2), (2.3) and (2.4) and obtain new displacements $\mathbf{u}(t+\Delta t)$. A more detailed scheme of the proposed approach is presented in Figure 2.4.

2.2 Validation of the mechanical model

In this section I validate my numerical scheme developed for the system of equations (2.1), (2.2), (2.3) and (2.4) describing quasi-static visco-elastic deformation of a Kelvin-Voigt body. I conduct my validation against a problem which has an exact solution. In this problem I consider a ho-

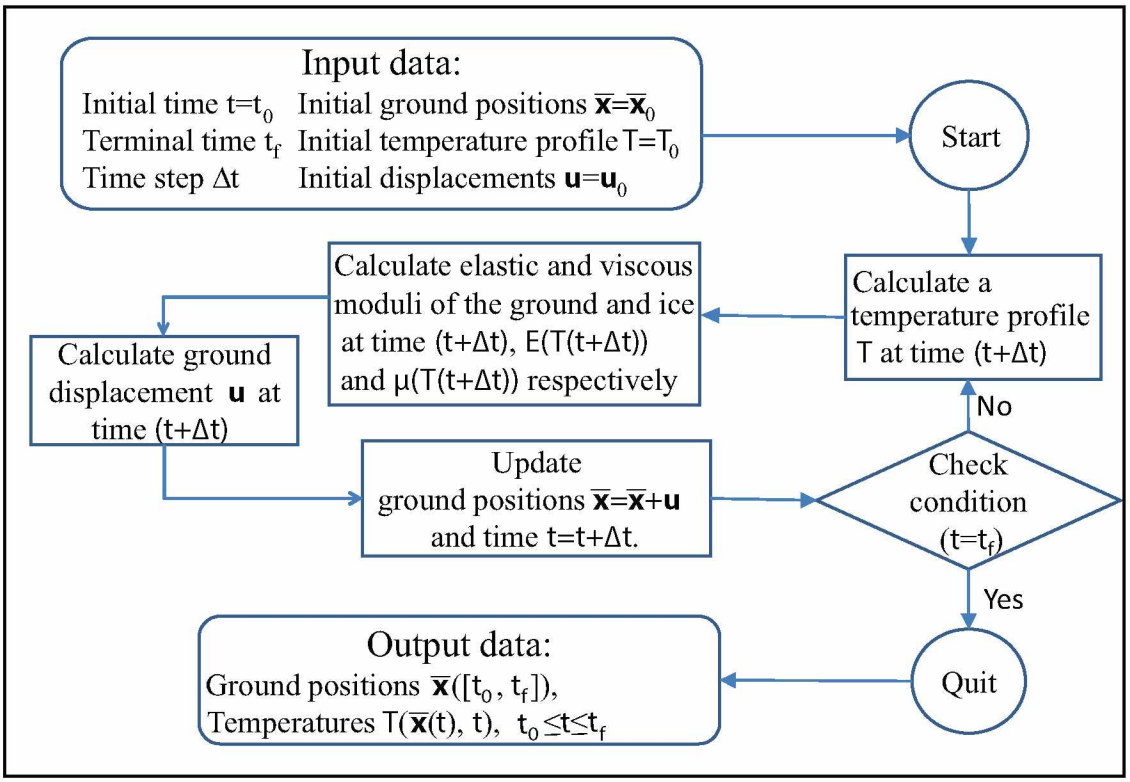

Figure 2.4: A scheme of the approach chosen for handling numerical solution of the heat equation coupled with the system of mechanical equations.

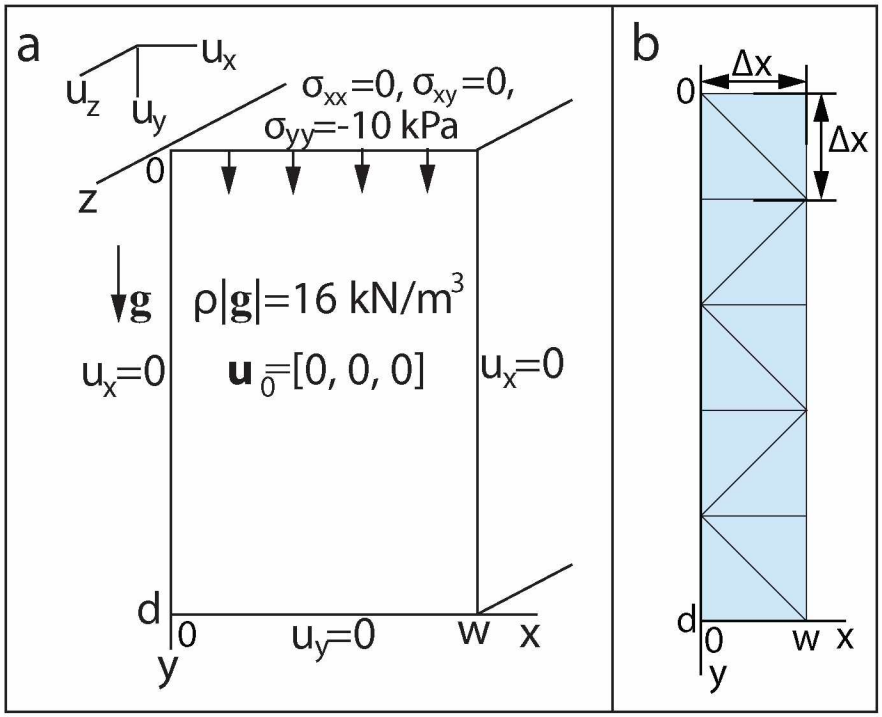

Figure 2.5: (a) A sketch of the computational domain for the problem of soil column subsidence. (b) An example of used computational grid with the grid size $\Delta x = 0.2$ m

mogeneous soil column which stands on the top of a non-deforming base. At an initial instant of time $t = 0$ this column is assumed to be non-deformed and to have a uniform mass density; elastic modulus E, viscosity μ and Poisson ratio ν of the soil are assumed to be uniform and constant. Deformation properties of the soil are described by the linear visco-elastic Kelvin-Voigt model (*Eringen*, 1980). At time $t = 0$ this column starts deforming because of the gravity force acting on it and a uniform load applied to its top.

To validate my numerical scheme I simulate a plane strain deformation of a $d = 1$ m tall soil column presented in Figure 2.5a. Volumetric weight $\rho|\mathbf{g}|$ of the undeformed soil is $16 \cdot 10^3$ N/m^3. The elastic modulus, the viscosity modulus and the Poisson's ratio for the soil are $2 \cdot 10^6$ Pa, $4 \cdot 10^{11}$ Pa $\cdot\, s$ and 0.3 respectively. A normal uniform stress $\boldsymbol{\sigma} = \begin{bmatrix} 0 & 0 & 0 \\ 0 & -10^4 & 0 \\ 0 & 0 & 0 \end{bmatrix}$ $[Pa]$ is applied at the top of the column. The column displacement in x- direction u_x for any instant of time is defined as zero. Deformation of the column is simulated over a time interval of 12 days. In this case, a total displacement of each point of the column at any instant of time can be calculated analytically. In my problem I numerically calculate displacements over a two-dimensional cross-section of the column. Then I compare produced numerical results for the displacements against the analytical solution which I derived utilizing a conception of the Henky strain (also called the logarithmic strain or the true strain) (*Xiao et al.*, 1997).

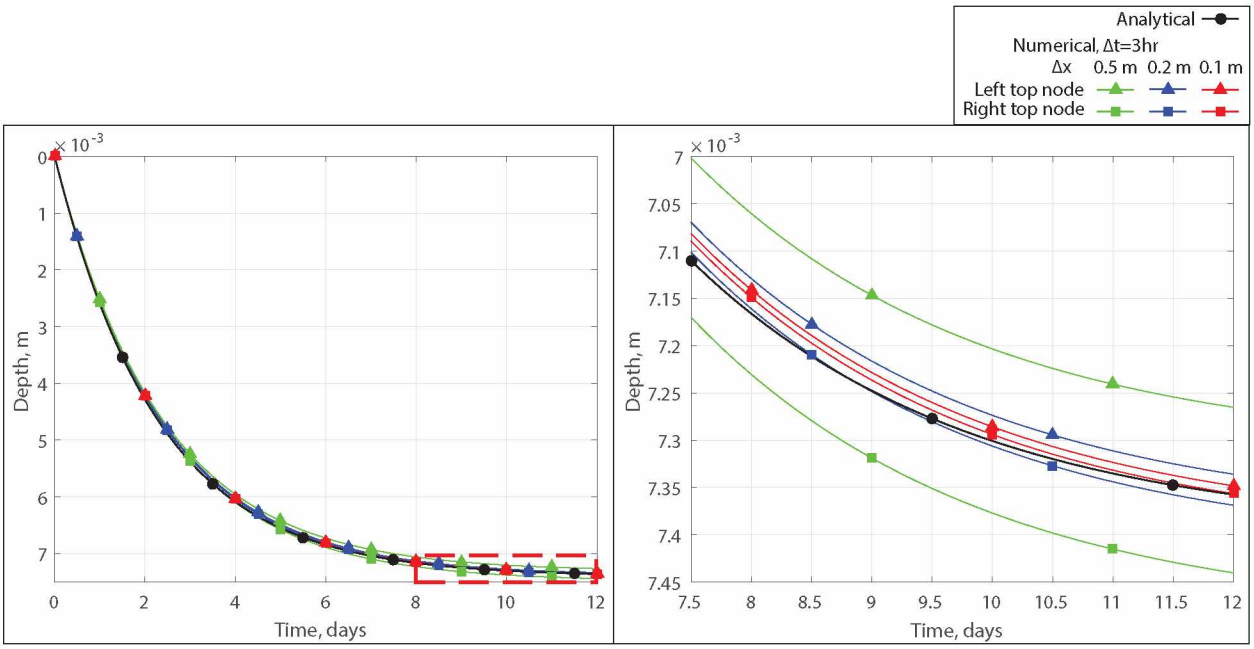

Figure 2.6: Displacements for the top of the column calculated over different grids and different nodes at the top of each grid.

I simulated the ground displacements over three different grids. Each grid has a uniform partition with grid size $\Delta x = 0.1,\ 0.2$ and 0.5 m. The width of the computational domain w for each grid is equal to its grid size. An example of a computational grid is presented in Figure 2.5b. For each grid simulations were handled with fixed time steps $\Delta t = 3$, 12, and 48 hours.

The analyses of the numerical solutions show that for each particular column there is a systematic difference between displacements for the left and for the right node presenting the top of the column. This difference does not significantly depend on a choice of the time step Δt, and can be explained by asymmetry of the grid partition. However, as shown in Figure 2.6 this difference decreases with reduction of grid size Δx. In Figure 2.7 I compare the numerical results for the top of the column against the analytical solution for different choices of time step Δt. Because of the bias associated with the choice of left or right node, I conduct comparisons for mean displacements of a top of a grid, calculated as averages of displacements for left and right nodes. Comparisons are conducted over the same grid with grid size $\Delta x = 0.1$ m, for which this bias is smallest. Plots shown in Figure 2.7 clearly demonstrate the convergence of numerical results for the top of the column to the exact solution with respect to time step Δt.

An error analysis for displacements over the entire column was also conducted and its results are listed in Table 2.1. Each value in the table represents a mean quadratic displacement error estimated over the entire column and the entire time of a simulated process. These results show that with a

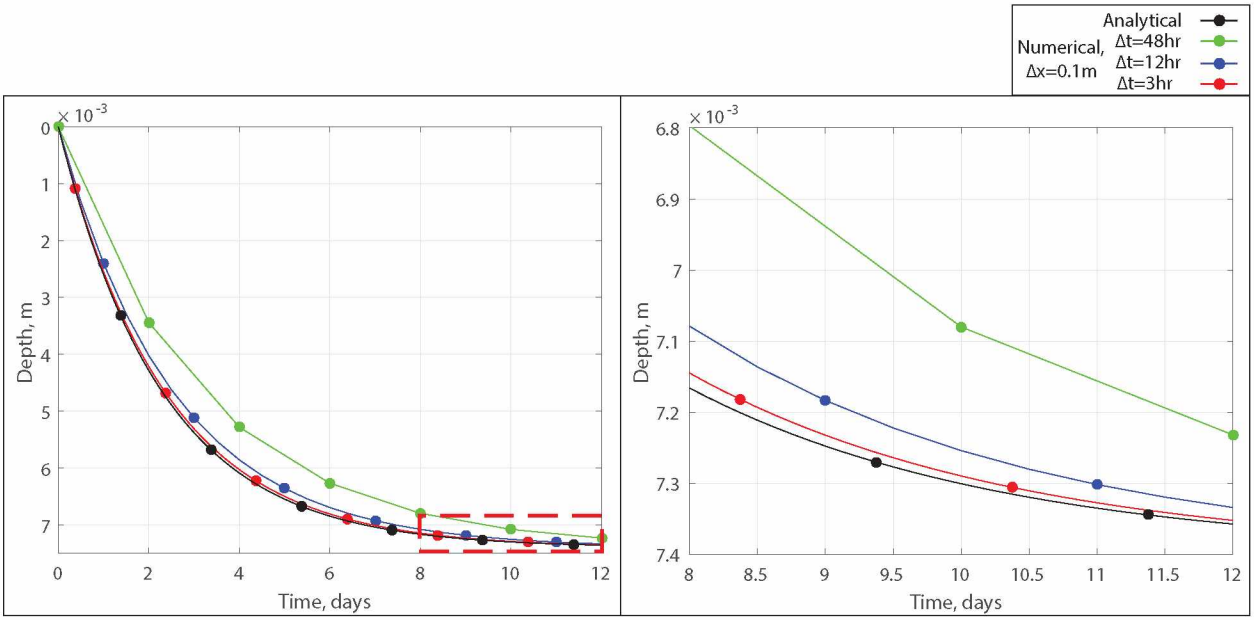

Figure 2.7: Mean displacements for the top of the column calculated for different times step dt over the same grid with the grid size $\Delta x = 0.1$ m.

Table 2.1: Discrepancies between the numerical and analytical solutions for the column subsidence. For each pair $\{\Delta x, \Delta t\}$ the discrepancy is estimated as $\max_{(x,y,t)}\{\mathbf{u}^{\text{num}} - \mathbf{u}^{\text{an}}\}$, where $\mathbf{u}^{\text{num}}$ and $\mathbf{u}^{\text{an}}$ are numerical and analytical solutions for displacements dynamics respectively. The errors are presented in 10^{-5}m.

$\Delta t/\Delta x$	0.5 m	0.2 m	0.1 m
48 hours	2.901	1.961	1.433
12 hours	0.487	0.286	0.208
3 hours	0.140	0.040	0.027

decrease of both time step Δt and grid size Δx errors rapidly decrease down to zero. This fact allows me to conclude that with decrease of both time step Δt and grid size Δx numerical solutions for the column consolidation converge to the exact solution and hence, my numerical scheme properly handles a plane strain problem for a Kelvin-Voigt material with a non-zero Poisson ratio.

2.3 Application of the coupled thermo-mechanical model to simulation of ice wedge degradation and trough formation

In this section I apply my developed thermo-mechanical model for simulation of the ice wedge degradation process. I assume that an ice wedge is buried into soil consisting of two homogeneous layers with uniform thermal and mechanical properties each. The ground is covered by seasonal snow, 30 cm deep at its maximum. The top of the ice wedge in my problem is located 40 cm under the ground surface. A detailed sketch for the problem is presented in Figure 2.8.

The heat equation (1.1) and the system of equations (2.1), (2.2), (2.3) and (2.4) describing temperature dynamics in the ground and snow and deformation of the ground respectively are solved over cross-sections presented in Figure 2.8 plots (a) and (c). In particular, Figure 2.8a shows a sketch for the thermal problem, solved by equation (1.1) and Figure 2.8c shows a sketch for the mechanical problem, solved by system of equations (2.1), (2.2), (2.3) and (2.4).

Here I would like to describe initial and boundary conditions for the temperature dynamics problem. I generated an initial ground temperature profile $T_0(x, y, t)$ for the cross-section shown in Figure 2.8a through simulation of 50 annual temperature cycles over a 30 m deep narrow soil column, with the same thermal properties as the ground at the center of the polygon. The air temperature above the soil column was changing as

$$T(t) = T_{m0} + A_0 \cdot \sin(2\pi/\tau t + \phi_0)$$

where $T_{m0} = -10°C$ is the mean annual temperature, $A_0 = 17K$ is the amplitude, $\tau = 365$ days is the one year period, and $\phi_0 = \pi$ is the initial phase, indicating that the simulation starts at the middle of autumn. A 30 cm thick layer of snow appears when the air temperature drops in autumn below $-7°C$ and disappears when the air temperature rises above $-2°C$ in the spring. Zero heat fluxes are prescribed at lower, left and right sides of the soil column. An initial temperature at the entire soil column was prescribed as $-5°C$ and was chosen to be close to a mean temperature at the ground surface. The mean annual temperature was chosen so that a maximal depth of simulated seasonal thawing at the center of the polygon was almost 40 cm, the depth for the top of the ice wedge located at another side of the cross-section. After generation temperature dynamics

at the center of the polygon, the ground temperature profile $T_0(x, y, t)$ for the entire cross-section containing the ice wedge was obtained through rescale of the temperature profile generated for the center of the polygon on the entire ground cross-section. So, I obtained temperature dynamics at the cross-section which would be close to temperature dynamics around a stable non-deforming ice wedge polygon. Then the air temperature above the entire cross-section has increased at some point and now is represented as

$$T_{air}(t) = T_m + A \cdot \sin(2\pi/\tau t + \phi),$$

where $T_m = -7.5°$ C is the mean annual temperature, $A = 17$ K is the amplitude, $\tau = 365$ days is the one year period, and $\phi = \pi$ is the initial phase, indicating that simulation over the ground cross-section starts in the middle of autumn. The 30 cm thick layer of snow appears when air temperature drops in autumn below $-7°C$ and disappears when the air temperature rises above $-2°C$ in spring. Because of symmetry assumptions described in Chapter 1 zero heat fluxes are prescribed on left and right boundaries of the cross-section. For simplicity zero heat flux is prescribed at the lower boundary at 30 m depth. I assign zero heat flux at the lower boundary because effects of natural temperature gradients existing at this depth on the active layer are negligible. Also, the effect of seasonal temperature variation on the ground surface is negligible at this depth and temperature gradients at this depth usually exist due to the geothermal heat flux and climate trends. Because of the geothermal heat flux mean annual ground temperatures are supposed to increase with depth. On the other hand due to the last decades of climate warming trends many observations record a decrease of ground temperatures with the depth. I cannot be always sure which trend dominates at the lower boundary and prescribing a zero value could be a good trade off between these trends.

Mechanical displacements in the ground are simulated over the upper layer of soil with the upper part of the ice wedge as shown in Figure 2.8c. The impact of the weight of seasonal snow cover on ground subsidence is assumed to be negligible and is not included in the simulation. Zero stress $\boldsymbol{\sigma}$ is prescribed at the ground surface, zero horizontal displacements $u_x = 0$ are prescribed at the left and right side of the domain and zero vertical displacement $u_y = 0$ is prescribed at the bottom. Deformation of the ground cross-section is considered as a plane strain problem: for each point of the domain zero frontal displacement $u_z = 0$ holds. At an initial instant of time the ground is assumed to be non-deformed: the condition $\mathbf{u}_0 = [0,\ 0,\ 0]$ is prescribed at the initial instant of time $t = 0$ at each point of the cross-section.

For computational efficiency snow cover is not even included into the mechanical domain and deformations are estimated only over the upper 0.8 m deep ground layer as shown in Figure 2.8c. A choice of this depth is based on a predicted maximal depth of seasonal thawing for this numerical

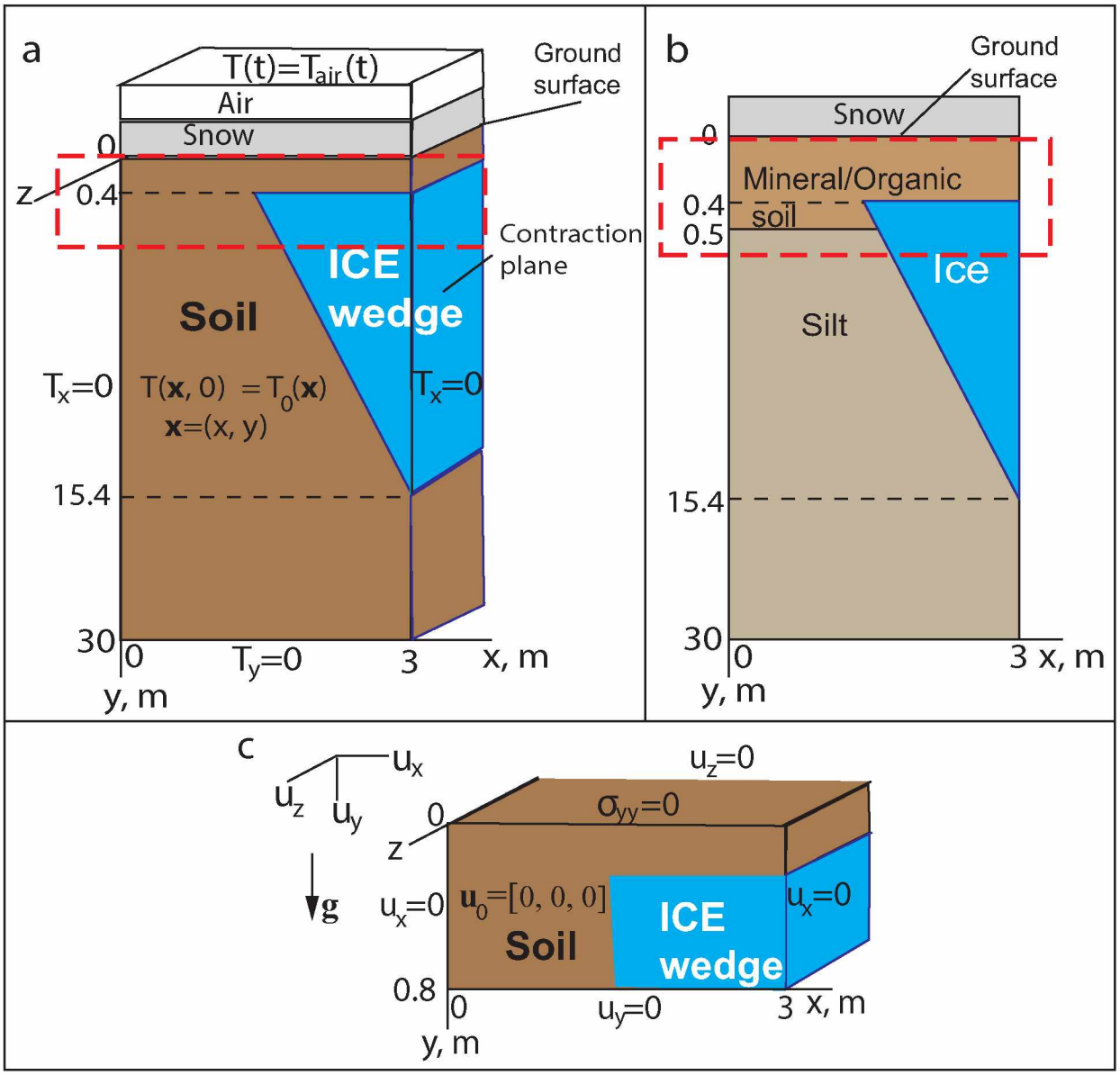

Figure 2.8: (a) A sketch of the temperature dynamics problem. (b) A scheme of ground layers, snow and ice in the entire 2-D cross-section. (c) A sketch of the mechanical problem.

experiment. This prediction was based on calculations made over a coarse numerical grid. From results of these calculations I am assured that below this depth the ground remains frozen year round and its possible deformations below this depth are negligible.

In Table 2.2 I describe detailed thermal and mechanical properties of the ground layers, ice wedge and snow considered in my problem. In my simulations for simplicity soil consists of a top mixed mineral/organic layer, and lower mineral layer known as silt. The presence of mixed mineral/organic layers in soil is typical for tundra and explained by cryoturbation processes typical for the active layer and the top of permafrost. My choices of thermal properties and water content for ground layers and thermal properties of snow are in particular based on results published in (*Nicolsky et al.*, 2009) and (*Smith*, 1975) and calibrated results presented in Table 1.3. Choices of mechanical properties for thawed ground layers such as elastic modulus and volumetric weight are based on properties published in (*Nicolsky et al.*, 2008) and (*Hossain et al.*, 2015) respectively. Choices of mechanical properties for ice are based on those published in (*Petrovic*, 2003). Elastic modula for frozen ground layers are chosen as intermediate between elastic modula for ice and thawed ground layers. Water appearing upon thawing of wedge ice is treated as an inelastic material which does not accumulate any internal stress and its mechanical properties are introduced into the model with the purpose of avoiding instability of the numerical scheme. Viscosity modula and Poisson's ratios for frozen ground layers were assumed to be the same as viscosity modulus and Poisson's ratio for ice. Choices of hypothetical viscosities for thawed ground layers and for water which appears upon melting of wedge ice are based on performance of numerical simulations and the rates of ground subsidence compared to the rates of melting of wedge ice. Too large values of viscosity for thawed ground and water would make the process of ground subsidence too slow, so its subsidence would not finish before autumn refreezing, at the same time too small viscosity values for thawed ground and water would lead to a drastic decrease of time steps, making performance of simulations too slow. Detailed thermo-mechanical properties of soil layers, snow and the ice wedge employed in the numerical solution are presented in Table 2.2.

In my experiment I would like to investigate effects of the snow cover, and the ground water table on a positive feedback between ice wedge degradation and trough formation. For this purpose I would like to consider 4 subproblems. In subproblem (i) the ground is assumed to be well-drained in summer with the ground water table height $h \equiv 0$. When seasonal snow covers the ground surface it entirely fills the forming trough so that the snow/air boundary is flat. The minimal thickness of the full snow cover is 30 cm. In subproblem (ii) the height of the ground water table is also $h \equiv 0$, however the depth of the snow cover every winter remains uniform across the cross-section so that every winter the shape of the snow/air boundary exactly reproduces the topography of the ground

Table 2.2: Thermal and mechanical properties of soil, wedge ice and snow in frozen and thawed states.

		Mineral/ Organic	Silt	Ice wedge	Snow
Depth of location, [m]		$0-0.5$	$0.5-30$	$0.4-15.4$	$-0.3-0$
Volumetric heat capacity, C [MJ/m^3]	Frozen	1.93	2.03	2.1	0.6
	Thawed	2.98	2.66	4.2	–
Thermal conductivity, λ [W/m $\cdot$ K]	Frozen	1.2	1.8	2.24	0.18
	Thawed	0.6	1.19	0.56	–
Porosity, η [m^3/m^3]		0.5	0.3	1	0
Unfrozen water parameters	a	0.001	0.001	0.001	–
	b	0.8	0.56	0.999	–
Freezing point depression, T^* [°C]		-0.01	-0.03	-0.001	–
Volumetric weight, $\rho\|\mathbf{g}\|$ [kN/m^3]		12	16	9	–
Elastic modulus, E [Pa]	Frozen	$3.2 \cdot 10^8$	$3.2 \cdot 10^7$	$1 \cdot 10^{11}$	–
	Thawed	$1 \cdot 10^6$	$1 \cdot 10^6$	0	–
Viscosity, μ $[Pa \cdot s]$	Frozen	$1 \cdot 10^{12}$	$1 \cdot 10^{12}$	$1 \cdot 10^{12}$	–
	Thawed	$1 \cdot 10^{12}$	$1 \cdot 10^8$	$1 \cdot 10^8$	–
Poisson ratio, ν		0.3	0.3	0.3	–

surface. The thickness of full snow cover is also 30 cm. In subproblem (*iii*) the seasonal snow cover is completely removed from the ground surface. The height of the ground water table like in the other two subproblems is also $h \equiv 0$. In subproblem (*iv*) like in subproblem (*i*) the seasonal snow cover completely fills the trough, forms a flat snow/air boundary, and the minimal thickness of full snow cover is 30 cm. However, the flat water table is present in the ground and located at the constant depth of 10 cm under the center of the ice wedge polygon.

2.4 Results and Limitations

In Figure 2.9 there are presented snapshots of troughs for subproblem (*i*) taken in autumn of each year. One can see a clear formation of the trough. Also, a top of a degrading wedge appears to become concave, and to resemble a shape of the above located trough. This fact is explained by uneven subsidence of ground into a water body which appears upon melting of the ice wedge. The non-uniform subsidence of the ground in summer can be explained by its elastic properties.

In Table 2.3 there are presented results for annual ground subsidence for all subproblems. One can notice in all simulations a rapid decline of the rate of the trough formation. This decline could be explained by the restrictive influence of ground elastic properties. Comparing results for ground subsidence in subproblems (*i*)-(*iii*) one can notice that these results are very similar to each other.

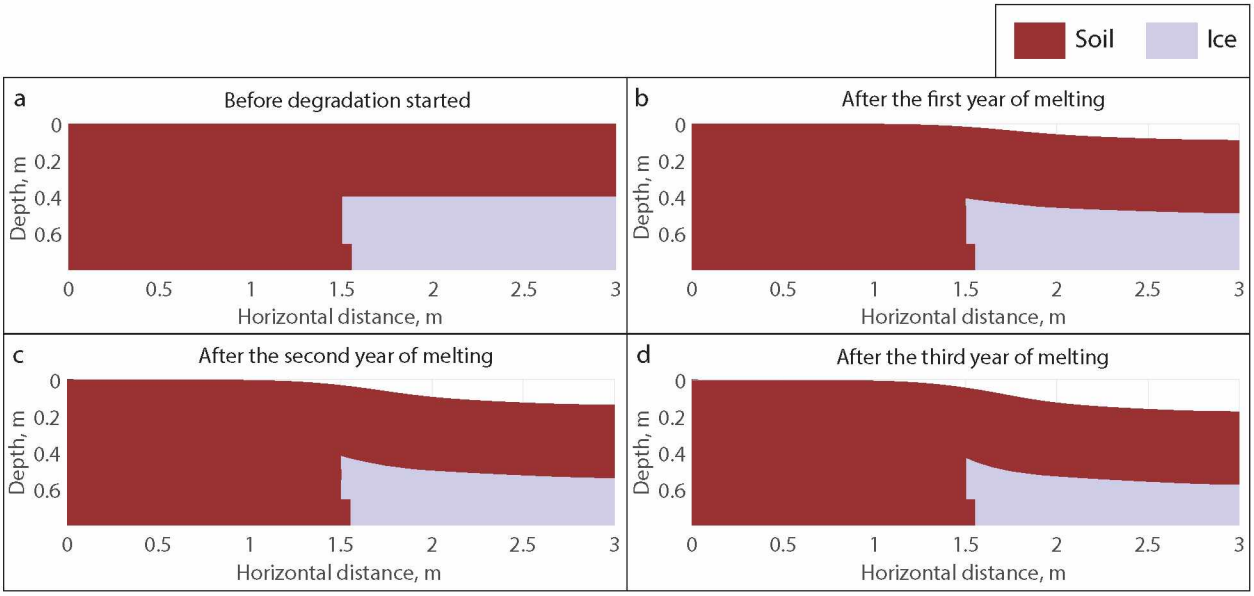

Figure 2.9: A top part of the ground cross-section containing the melting ice wedge in subproblem (i). (a) Before melting started. (b) After the first year of melting. (c) After the second year of melting. (d) After the third year of melting.

Table 2.3: Annual displacement dynamics for the ground surface at the forming trough and at the center of the ice wedge polygon. The results are presented for different subproblems. In subproblems (i)-(iii) there is no ground water table assumed. In subproblem (i) the snow cover above the cross-section has a flat surface at the top with the minimal thickness of 30 cm. In subproblem (ii) the snow cover has a uniform thickness of 30 cm. In subproblem (iii) the snow cover is absent. In subproblem (iv) the snow is distributed in the same way as in subproblem (i) and the water table at 10 cm under the center of the ice wedge polygon is present.

		Subproblem			
	Year	(i)	(ii)	(iii)	(iv)
Vertical ground displacement above the ice wedge, cm	1	9.03	9.03	7.46	5.17
	2	13.96	13.86	12.63	8.00
	3	17.64	17.52	16.12	9.41
Vertical ground offset at the center of the polygon, cm	1	0.18	0.18	0.15	0.08
	2	0.35	0.35	0.30	0.15
	3	0.54	0.53	0.44	0.23
Ground subsidence above the ice wedge with removed offset, cm	1	8.85	8.85	7.30	5.09
	2	13.60	13.51	12.33	7.84
	3	17.09	16.99	15.69	9.18
Difference in ground subsidence above the ice wedge between current and previous year with removed offsets, cm	1	8.85	8.85	7.30	5.09
	2	4.76	4.66	5.03	2.75
	3	3.49	3.48	3.35	1.34

Definitely, partial and full removals of snow cover seem to reduce the process of trough formation but their contribution does not seem significant. From these results I conclude that in my problem the effect of snow cover on a positive feedback between ice wedge degradation and trough formation is not significant. On the other hand, rates of trough formation in subproblems (*i*)-(*iii*) are much greater than the rate in subproblem (*iv*) where the ground water table is present. It shows that the water table in my thermo-mechanical problems has a significant restrictive effect on the ground subsidence and the trough formation. It implies that in a natural environment in poorly drained areas melting of tops of ice wedges may lead to very small ground deformations or no deformations at all. On the other hand, poor drainage of the areas may lead to the presence of water in forming troughs. Appeared water would necessarily change the heat transfer process between air and the underlying ice wedge and lead to formation of a thermokarst pond above a rapidly degrading ice wedge. Unfortunately, my thermo-mechanical model is not applicable for this case. So, my model is applicable only for the cases when there is no water staying in forming troughs.

Besides vertical ground displacements for the center of the trough for each year, my data include systematic offsets of the ground at the center of the polygon. This systematic offset appears because my model reproduces the process of summer soil consolidation associated with reduction of the elastic modulus upon thawing but it does not reproduce the process of soil expansion upon freezing which is associated with seasonal heaving and water expansion in pores. My attempts to reproduce the soil expansion were not successful because due to large stresses mechanical deformation was unstable and large errors were produced. At the same time the elastic properties and the porosity of the ground in my model do not change upon soil consolidation. The presence of this systematic error and simplification of the process imply that my model is applicable only for a short term simulation of a trough development.

Many field observations show ground cracks in forming troughs. Ground cracking leads to changes in the processes of heat transfer and deformation. In my numerical model ground cracking is not considered at all. Also, even if the ground does not fracture, its visco-elasto-plastic properties may change upon its deformation and these changes are also not considered in my model, as well as plastic deformation which is not considered at all. Soil mechanical properties may sustain significant variations if large loads caused by vehicles or constructions are applied to the ground.

From all these facts I conclude that my numerical model can be applied for simulation of ice wedge degradation and trough formation only at initial stage, lasting for several years. Moreover, it is applicable only for natural tundra landscapes where no external loads are applied to soil. It might also not apply for areas with very poor drainage or no drainage at all, where thermokarst depressions would easily lead to formation of ponds.

Conclusion

In this thesis, in Chapter 1 I numerically implemented a thermal model predicting temperature dynamics in the soil around stable nondegrading ice wedges. The temperature dynamics were predicted through simulation of heat conduction with phase change. I validated the thermal model against analytical solutions to the temperature waves problem and the Stefan problem. I observed that with a decrease of the grid size and a time step numerical results converge on results predicted analytically. It allowed me to conclude that the developed thermal model properly handles the processes of heat conduction and phase change. After validation I applied my thermal model for simulation of temperature dynamics to an ice wedge polygon located East of Barrow, Alaska. Despite a simplification of the heat transfer process in the model and oversimplifications of thermal properties of the ground and snow the numerically predicted results appeared to be more or less close to measurements. Some discrepancies between predicted and observed results were caused by oversimplified parametrization of the ground and snow properties and as we showed, it can be overcome without any change of the model. In Chapter 2, I updated my model adding to it a mechanical part predicting dynamics of ground deformation around an ice wedge melting due to increased air and ground temperatures. In particular I developed and validated a mechanical model describing deformation of a Kelvin-Voigt body. The mechanical model was combined with the thermal model developed in Chapter 1 into a thermo-mechanical model describing ice wedge temperature dynamics, ice wedge degradation and trough formation. The mechanical model was validated against an analytical solution to a problem in which consolidation of a soil column with non-zero Poisson ratio under gravity and external loads was considered. I observed that with a decrease of the grid size and a time step numerical results converge on results predicted analytically. It allowed me to conclude that the mechanical model properly handles the process of deformation of a Kelvin-Voigt body driven by external loads and the gravity force. After validation of the mechanical model, I applied my combined thermo-mechanical model for a simulation of trough formation. From calculation results I noticed that shapes of simulated troughs were resembling shapes of observed troughs above ice wedges. Also, a concave shape of a top of a simulated degrading ice wedge resembles shapes of tops of observed ice wedges. So, I found that the combined model reproduces well the main effects of the initial stage of an ice wedge degradation. Imposing different conditions for snow cover and height of the water table, I considered effects of the snow cover and the water table on the process of ice wedge degradation. I found that an additional snow cover contributed to a more rapid trough formation, however this contribution was not significant. On the other hand, the ground water table significantly affected the process of trough formation, making it much slower.

References

Bingham, E. C. (1916), An investigation of the laws of plastic flow, *Bulletin of the Bureau of Standards*, *13*, 309–353.

Bockheim, J. G., and K. M. Hinkel (2004), Characteristics and significance of the transition zone in drained thaw-lake basins of the Arctic Coastal Plain, Alaska, *Arctic*, *68*, 1002–1011.

Bowden, W., M. N. Gooseff, A. Balser, A. Green, B. J. Peterson, and J. Bradford (2008), Sediment and nutrient delivery from thermokarst features in the foothills of the North Slope, Alaska: Potential impacts on headwater stream ecosystems, *Journal of Geophysical Research: Biogeosciences*, *113*(G2).

Brewer, M. C. (1958), Some results of geothermal investigations of permafrost in northern Alaska, *Transactions, American Geophysical Union*, *39*(1), 19–26.

Burn, C. R., and A. G. Lewkowicz (1990), Canadian landform examples-17 retrogressive thaw slumps, *The Canadian Geographer/Le Géographe canadien*, *34*(3), 273–276.

Carslaw, H., and J. Jaeger (1959), *Conduction of Heat in Solids*, Oxford University Press, London.

Comini, G., S. D. Giudice, and O. Saro (1989), Conservative equivalent heat capacity methods for non-linear heat conduction, *Numerical Methods in Thermal Problems*, *6*(Part 1), 5–15.

Côté, J., M. Rahimi, and J. Konrad (2012), Thermal conductivity of compacted snow, in *Cold Regions Engineering 2012: Sustainable Infrastructure Development in a Changing Cold Environment*, pp. 833–843, ASCE.

Davis, N. (2001), *Permafrost: A Guide to Frozen Ground in Transition*, University of Alaska Press, Fairbanks, Alaska.

de K. Leffingwell, E. (1915), Ground-ice wedges: The dominant form of ground-ice on the north coast of Alaska, *The Journal of Geology*, *23*, 635–654.

de Vries, D. (1963), *Physics of the Plant Environment, chap. Thermal properties of soils*, pp. 210–235, Wiley, New York.

Dienes, J. K. (1979), On the analysis of rotation and stress rate in deforming bodies, *Acta Mechanica*, *32*(4), 217–232.

Drucker, D. C., and W. Prager (1952), Soil mechanics and plasticity analysis of limit design, *Quarterly of Applied Mathematics*, *10*(2), 157–165.

Eringen, A. C. (1980), *Mechanics of Continua*, Robert E. Krieger Publishing Co.,, Huntington, NY.

Erwin, S. (1963), Origin of ice wedges, in *Proceedings. Permafrost International Conference*, Publication No. 1287, pp. 82–87, National Academy of Sciences - National Research Council, Washington, D.C.

Fortier, D., M. Allard, and Y. Shur (2007), Observation of rapid drainage system development by thermal erosion of ice wedges on Bylot island, Canadian Arctic Archipelago, *Permafrost and Periglacial Processes*, *18*(3), 229–243.

Galushkin, Y. (1997), Numerical simulation of permafrost evolution as a part of sedimentary basin modeling: permafrost in the Pliocene - Holocene climate history of the Urengoy field in the West Siberian basin, *Canadian Journal of Earth Sciences*, *34*, 935–948.

Gambolati, G., M. Ferronato, P. Teatini, R. Deidda, and G. Lecca (2001), Finite element analysis of land subsidence above depleted reservoirs with pore pressure gradient and total stress formulations, *International journal for numerical and analytical methods in geomechanics*, *25*(4), 307–327.

Glowinski, R., T.-W. Pan, and J. Periaux (1994), A fictitious domain method for Dirichlet problem and applications, *Computer Methods in Applied Mechanics and Engineering*, *111*(3-4), 283–303.

Goodrich, L. E. (1982), The influence of snow cover on the ground thermal regime, *Canadian Geotechnical Journal*, *19*, 421–432.

Gupta, S. (2003), *The Classical Stefan Problem*, 404 pp., Elsevier, Amsterdam.

Hinzman, L. D., D. J. Goering, S. Li, and T. C. Kinne (1997), Numeric simulation of thermokarst formation during disturbance, *Disturbance and Recovery in Arctic Lands: An Ecological Perspective, Kluwer Academic Publishers, Dordrecht, The Netherlands*, p. 621.

Hobbs, P. (1974), *Ice Physics*, Claredon Press, Oxford.

Holzapfel, G. A. (2000), *Nonlinear Solid Mechanics: A Continuum Approach for Engineering*, John Wiley and Sons.

Hossain, M. F., W. Chen, and Y. Zhang (2015), Bulk density of minear and organic soils in the Canada's arctic and sub-arctic, *Information processing in agriculture*, *2*, 183–190.

Jafarov, E. E., V. E. Romanovsky, H. Genet, A. D. McGuire, and S. S. Marchenko (2013), The effects of fire on the thermal stability of permafrost in lowland and upland black spruce forests of Interior Alaska in a changing climate, *Environmental Research Letters*, *8*(3), 035,030.

Jafarov, E. E., D. J. Nicolsky, V. E. Romanovsky, J. E. Walsh, S. K. Panda, and M. C. Serreze (2014), The effect of snow: How to better model ground surface temperatures, *Cold Regions Science and Technology*, *102*, 63–77.

Jorgeson, M. T., Y. L. Shur, and E. R. Pullman (2006), Abrupt increase in permafrost degradation in Arctic Alaska, *Geophysical Research Letters*, *33*(2).

Kelley, C. (2003), *Solving Nonlinear Equations with Newton's Method*, No 1 in Fundamentals of Algorithms, SIAM.

Kolmogorov, A., and S. Fomin (1975), *Introductory Real Analysis*, Prentice-Hall, New York.

Lachenbruch, A. (1963), Contraction theory of ice-wedge polygons: a qualitative discussion, in *Proceedings. Permafrost International Conference*, Publication No. 1287, pp. 63–71, National Academy of Sciences - National Research Council, Washington, D.C.

Lantz, T. C., and S. V. Kokelj (2008), Increasing rates of retrogressive thaw slump activity in the Mackenzie Delta region, NWT, Canada, *Geophysical Research Letters*, *35*(6).

Lewis, K., G. Zyvoloski, B. Travis, C. Wilson, and J. Rowland (2012), Drainage subsidence associated with Arctic permafrost degradation, *Journal of Geophysical Research: Earth Surface*, *117*(F4).

Lewkowicz, A. G. (2007), Dynamics of active-layer detachment failures, Fosheim peninsula, Ellesmere island, Nunavut, Canada, *Permafrost and Periglacial Processes*, *18*(1), 89–103.

Liljedahl, A., L. Hinzman, and J. Schulla (2012), Ice-wedge polygon type controls low-gradient watershed-scale hydrology., in *Proceedings of the Tenth International Conference on Permafrost*, pp. 231–236.

Lunardini, V. J. (1988), Freezing of soil with an unfrozen water content and variable thermal properties, *Report 88-2*, Cold Region Research and Engineering Laboratory, US Army Cold Regions Research and Engineering Lab.

Luo, Z.-J., and Z. Feng (2011), Finite element numerical simulation of land subsidence and groundwater exploitation based on visco-elastic-plastic Biot's consolidation theory, *Journal of Hydrodynamics, Ser. B*, *23*(5), 615–624.

Mackay, J. R. (1974), Ice-wedge cracks, Garry island, Northwest territories, *Canadian Journal of Earth Sciences*, *11*, 1366–1383.

McGraw, M. (2008), The degradation of ice wedges in the Colville River Delta and their role in pond drainage, in *Ninth International Conference on Permafrost*, vol. 2, pp. 1161–1166.

Mölders, N., and V. E. Romanovsky (2006), Long-term evaluation of the hydro-thermodynamic soil-vegetation scheme's frozen ground/permafrost component using observations at Barrow, Alaska, *Journal of Geophysical Research*, *111*, D04,105.

Morgan, K., R. Lewis, and O. Zienkiewicz (1978), An improved algorithm for heat conduction problems with phase change, *International Journal for Numerical Methods in Engineering*, *12*(7), 1191–1195.

Nicolsky, D., V. Romanovsky, and G. Tipenko (2007a), Using in-situ temperature measurements to estimate saturated soil thermal properties by solving a sequence of optimization problems, *The Cryosphere*, *1*, 41–58.

Nicolsky, D., V. Romanovsky, and G.G.Panteleev (2009), Estimation of soil thermal properties using in-situ temperature measurements in the active layer and permafrost, *Cold Regions Science and Technology*, (55), 120–129.

Nicolsky, D. J., V. E. Romanovsky, V. A. Alexeev, and D. M. Lawrence (2007b), Improved modeling of permafrost dynamics in a GCM land-surface scheme, *Geophysical Research Letters*, *34*(L08501).

Nicolsky, D. J., V. E. Romanovsky, G. Tipenko, and D. Walker (2008), Modeling biogeophysical interactions in nonsorted circles in the Low Arctic, *Journal of Geophysical Research*, *113*(G03S05).

Osterkamp, T. E. (1987), Freezing and thawing of soils and permafrost containing unfrozen water or brine, *Water Resources Research*, *23*(12), 2279–2285.

Osterkamp, T. E., D. C. Esch, and V. E. Romanovsky (1997), *Implications of Global Change in Alaska and the Bering Sea Region - University of Alaska Fairbanks Workshop 1997*, chap. 10, pp. 115–118, BESIS Project Office, University of Alaska Fairbanks, Fairbanks, Alaska.

Osterkamp, T. E., M. T. Jorgenson, E. A. G. Schuur, Y. L. Shur, M. Z. Kanevskiy, J. G. Vogel, and V. E. Tumskoy (2009), Physical and ecological changes associated with warming permafrost and thermokarst in Interior Alaska, *Permafrost and Periglacial Processes*, *20*(3), 235–256.

Petrovic, J. J. (2003), Review mechanical properties of ice and snow, *Journal of materials science*, *38*, 1–6.

Pewe, T. L. (1963), Ice-wedges in alaska - classification, distribution, and climatic significance, in *Proceedings. Permafrost International Conference*, Publication No. 1287, pp. 76–81, National Academy of Sciences - National Research Council, Washington, D.C.

Pham, Q. (1986), The use of lumped capacitance in the finite-element solution of heat conduction problems with phase change, *International Journal of Heat and Mass Transfer*, *29*(2), 285–291.

Pham, Q. (1995), Comparison of general purpose finite element methods for the Stefan problem, *Numerical Heat Transfer Part B - Fundamentals*, *27*(4), 417–435.

Plug, L., and J. West (2009), Thaw lake expansion in a two-dimensional coupled model of heat transfer, thaw subsidence, and mass movement, *Journal of Geophysical Research: Earth Surface*, *114*(F1).

Qi, J., X. Yao, F. Yu, and Y. Liu (2012), Study on thaw consolidation of permafrost under roadway embankment, *Cold Regions Science and Technology*, *81*, 48–54.

Raynolds, M. K., et al. (2014), Cumulative geoecological effects of 62 years of infrastructure and climate change in ice-rich permafrost landscapes, Prudhoe Bay oilfield, Alaska, *Global Change Biology*, *20*(4), 1211–1224, doi:10.1111/gcb.12500.

Romanovsky, V. E., and T. E. Osterkamp (2000), Effects of unfrozen water on heat and mass transport processes in the active layer and permafrost, *Permafrost and Periglacial Processes*, *11*, 219–239.

Sass, J., A. Lachenbruch, and R. Munroe (1971), Thermal conductivity of rocks from measurements on fragments and its application to heat-flow determinations, *Journal of Geophysical Research*, *76*(14), 3391–3401.

Schaefer, K., H. Lantuit, V. E. Romanovsky, and E. A. G. Schuur (2012), Policy implications of warming permafrost., *United nations environment programme special report.*

Serreze, M., et al. (2000), Observational evidence of resent change in the northern high-latitude environment, *Climatic Change*, *46*, 159–207.

Smith, M. W. (1975), Microclimatic influences on ground temperatures and permafrost distribution, Mackenzie Delta, Northwest Territories, *Canadian Journal of Earth Sciences*, *12*, 1421–1438.

Tikhonov, A., and A. Samarskii (1963), *Equations of Mathematical Physics*, 765 pp., Pergamon Press LTD., Oxford, England.

USARC, U. A. R. C. (2003), Climate change, permafrost, and impacts on civil infrastructure, *Special report*, pp. 01–03.

Walther, G.-R., E. Post, P. Convey, A. Menzel, C. Parmesan, T. J. Beebee, J.-M. Fromentin, O. Hoegh-Guldberg, and F. Bairlein (2002), Elocogical responses to recent climate change, *Nature*, *416*, 389–395, doi:10.1038/416389a.

Walvoord, M., and R. G. Striegl (2007), Increased groundwater to stream discharge from permafrost thawing in the Yukon River basin: Potential impacts on lateral export of carbon and nitrogen, *Geophysical Research Letters*, *34*(12).

Wang, L., W. Wang, and F. Yu (2015a), Thaw consolidation behaviours of embankments in permafrost regions with periodical temperature boundaries, *Cold Regions Science and Technology*, *109*, 70–77.

Wang, S., J. Qi, F. Yu, and X. Yao (2013), A novel method for estimating settlement of embankments in cold regions, *Cold Regions Science and Technology*, *88*, 50–58.

Wang, W., L. Wang, F. Yu, and Q. Wang (2015b), One dimensional thaw consolidation behaviors with periodical thermal boundaries, *KSCE Journal of Civil Engineering*, pp. 1–9.

Wen, Z., Z. Yang, Q. Yu, D. Wang, W. Ma, F. Niu, Z. Sun, and M. Zhang (2016), Modeling thermokarst lake expansion on the Qinghai-Tibetan Plateau and its thermal effects by the moving mesh method, *Cold Regions Science and Technology*, *121*, 84–92.

West, J., and L. Plug (2008), Time-dependent morphology of thaw lakes and taliks in deep and shallow ground ice, *Journal of Geophysical Research: Earth Surface*, *113*(F1).

Xiao, H., O. T. Bruhns, and A. Meyers (1997), Logaritmic strain, logaritmic spin and logarithmic rate, *Acta Mechanica*, *124*, 89–105.

Yao, X., J. Qi, and W. Wu (2012), Three dimensional analysis of large strain thaw consolidation in permafrost, *Acta geotechnica*, *7*(3), 193–202.

Zhang, Q., V. E. Romanovsky, and A. D. McGuire (2001), Incorporation of a permafrost model into a large-scale ecosystem model: Evaluation of temporal and spatial scaling issues in simulating soil thermal dynamics, *Journal of Geophysical Research*, *106*(D24), 33,649–33,670.

Zienkiewicz, O., and R. Taylor (1991), *The Finite Element Method*, vol. 1, McGraw-Hill, London.

Zolotarevskaya, D. I. (2003), Mathematical modeling of the processes of deformation of soils with time, *Journal of engineering physics and thermophysics*, *76*(3), 632–639.